Pekka Röyttä

Study of a vapor-compression air-conditioning system for jetliners

Thesis for the degree of Doctor of Science (Technology) to be presented with due permission for public examination and criticism in the Auditorium 1383 at Lappeenranta University of Technology, Lappeenranta, Finland on the 4th of November, 2009, at noon.

Acta Universitatis Lappeenrantaensis
356

Supervisor Professor Jari Backman
Laboratory of Heat and Fluid dynamics
Department of Energy and Environmental Technology
Lappeenranta University of Technology
Finland

Reviewers Associate Professor Piero Colonna
Process and Energy Department
Delft University of Technology
Netherlands

Associate professor Andrew Martin
Department of Energy Technology
Royal Institute of Technology
Sweden

Opponents Associate Professor Piero Colonna
Process and Energy Department
Delft University of Technology
Netherlands

Associate professor Andrew Martin
Department of Energy Technology
Royal Institute of Technology
Sweden

ISBN 978-952-214-832-2
ISBN 978-952-214-833-9 (PDF)
ISSN 1456-4491
Lappeenrannan teknillinen yliopisto
Digipaino 2009

Abstract

Pekka Röyttä
Study of a vapour-compression air-conditioning system for jetliners
Lappeenranta 2009
128 pages
Acta Universitatis Lappeenrantaensis 356
Diss. Lappeenranta University of Technology
ISBN 978-952-214-832-2, ISBN 978-952-214-833-9 (PDF), ISSN 1456-4491

Most modern passenger aeroplanes use air cycle cooling. A high-speed air cycle is a reliable and light option, but not very efficient. This thesis presents research work done to design a novel vapour cooling cycle for aeroplanes. Due to advancements in high-speed permanent magnet motors, the vapour cycle is seen as a competitive option for the air cycle in aeroplanes. The aerospace industry places tighter demands on the weight, reliability and environmental effects of the machinery than those met by conventional chillers, and thus modifications to conventional design are needed.

The thesis is divided into four parts: the initial screening of the working fluid, 1-D design and performance values of the compressor, 1-D off-design value predictions of the compressor and the 3-D design of the compressor.

The R245fa was selected as the working fluid based the study. The off-design range of the compressor was predicted to be wide and suitable for the application. The air-conditioning system developed is considerably smaller than previous designs using centrifugal compressors.

Keywords: vapour cooling cycle, centrifugal compressor, high-speed, aeroplanes
UDC 621.564 : 621.57 : 621.515 : 629.7.06 : 004.942

Acknowledgements

This study was carried out in the department of Energy and Environmental Technology at Lappeenranta University of Technology, Finland, between 2006 and 2009.

First of all, I would like to express my sincere gratitude to my supervisor and instructor Professor Jari Backman for all the valuable comments and support he provided during this study.

I would also like to thank professor Jaakko Larjola for his work and guidance on the project in which this dissertation was mostly made. I also extend my gratitude to all of my coauthors.

I grateful for the reviewers of this thesis, professors Piero Colonna and Andrew Martin. Their suggestions and insight on the subject have helped greatly to improve the work.

This work was supported by MOET-project, an EU FP 6 project, the Finnish Funding Agency for Science and Technology, and The Finnish Cultural Foundation in South Karelia .

Pekka Röyttä
March 2009
Lappeenranta, Finland

To Riikka

Contents

List of publications

Publication I
Röyttä P., Honkatukia J. and Turunen-Saaresti T. Centrifugal Compressor Working Fluids for Refrigeration Cycle *In proceedings of ASME 2009 Gas Turbine Technical Congress*

The candidate was the corresponding author and did the simulations with some help from Mr. Honkatukia. The candidate wrote the paper together with Mr Honkatukia and Dr Turunen-Saaresti.

Publication II
Röyttä P., Turunen-Saaresti T. and Honkatukia J. Optimising the refrigeration cycle with a two-stage centrifugal compressor and a flash intercooler. *International Journal of Refrigeration, Volume 32, Issue 6, September 2009, Pages 1366-1375*

The candidate is the corresponding author of the paper. Dr Turunen-Saaresti developed the code with a contributions from the candidate and Mr Honkatukia. The candidate did the simulations. This paper was written by the candidate, Dr Turunen-Saaresti and Mr Honkatukia in collaboration.

Publication III
Turunen-Saaresti T., Röyttä P., Honkatukia J. and Backman J. Predicting off-design range and performance of refrigeration cycle with two-stage centrifugal compressor and flash intercooler, *International Journal of Refrigeration* Submitted for publication

Dr Turunen-Saaresti is the corresponding author. The candidate wrote about the compressor map and efficiency prediction, and took part in analysing the results. Mr Honkatukia provided the algorithms.

Publication IV
Röyttä P., Grönman,A., Jaatinen A., Turunen-Saaresti T. and Backman J. Improving centrifugal compressor impeller channel shape and length, *International Journal of Rotating Machinery,* Submitted for publication

The candidate is the corresponding author of the paper. The research idea was candidates. The simulations were done by Messrs Grönman and Jaati-

nen. The results were analysed by the candidate and Messrs Grönman and Jaatinen. Dr Turunen-Saaresti gave valuable comments on the numerical modelling and results.

Nomenclature

Abbreviations

CFD	computational fluid dynamics
COP	coefficient of performance
GWP	global warming potential

Latin alphabet

A	area	m^2
a	speed of sound	m/s
b	Blade height at trailing edge	m
C_f	friction coefficient	–
C_{pr}	static pressure rise coefficient	-
d	diameter	m
l	length of flow passage	m
h	specific enthalpy	J/kg
k	loss coefficient	-
k_1	roughness coefficient	–
k_2	velocity factor	–
K_p	pressure loss coefficient	-
K_{rel}	relative surface roughness	–
M	Mach number	–
N_s	specific speed	–
P	circumference	m
p	pressure	Pa
q_m	mass flow	kg/s
q_v	volumetric flow	m^3/s
r	radius	m
k	loss coefficient	-
T	temperature	K
U	peripheral velocity	m/s
V	relative flow velocity	m/s
$\dot{W}$	power	W
x	vapour content	–

Dimensionless numbers

Re	Reynolds number	–

Greek alphabet

Δ	change	–
η	efficiency	-
μ	dynamic viscosity	$\mathrm{Pa} \cdot \mathrm{s}$
ω	angular speed	rad/s
ϕ	heat flux	W
π	pressure ratio	–
ψ	loading coefficient	–
ρ	density	$\mathrm{kg/m^3}$
ξ	friction coefficient	–

Subscripts

1	compressor inlet
2	impeller outlet
3	diffuser outlet
af	tangential acceleration friction losses
bearing	bearings
b	blade height
c1	1^{st} stage compressor
c2	2^{nd} stage compressor
c	condensation
cool	cooling
des	design point
dh	hydraulic diameter
e	evaporation
ec	electric motor cooling losses
el	electrical
flash	flash intercooler
gf	gas friction losses
g	gas
h	hydraulic
l	liquid
le	impeller blade leading edge
max	maximum
M	motor losses
r	rotor
s	isentropic
sl	shape loss
t	total
t-t	total to total

th	thermal
tip	blade tip

Chapter 1

Introduction

The goal of the work documented in this thesis is the study of the feasibility of an air-conditioning system for airliners based on a vapour-compression thermodynamic cycle. This study considers high-speed centrifugal compressors, the selection of the working fluid and the cycle configuration. The work is divided into four parts, screening the possible working fluids for the thermodynamic cycle, 1-D design and optimisation of the thermodynamic cycle, 1-D off-design modelling of the thermodynamic cycle, and studying the 3-D geometry of the compressor.

The basis of a feasibility study of a high-speed centrifugal compressor-powered vapour cooling cycle in aeromotive use is laid down in the study. Based on the results of this study a working prototype of the thermodynamic cycle was build.

To be able to model the performance of a thermodynamic cycle some initial values, such as cooling capacity, evaporation temperature and condensation temperature had to be set at the beginning of the project. Unfortunately, due to the wishes of the customer, the evaporating temperature and cooling capacity had to be changed during project between publications I and II. This makes comparing the results of the initial screening of working fluids, presented in publication I, to the actual design somewhat hard. After the initial screening of the working fluid two candidates, R134a and R245fa, were chosen for closer inspection at more detailed system calculations presented in publication II.

The compressor was designed and modelled with computational fluid dynamics (CFD). The compressor maps were produced from the results of this modelling. According to our previous experience, the shape of the speed lines of the compressor maps is correct but efficiency is somewhat over predicted by the CFD. Accordingly, have introduced correction factors for the efficiency. These maps together with the system configuration were combined into a

simulation showing the cooling power range of this specific thermodynamic cycle. This is presented in publication III. On the basis of these studies the R245fa was chosen as the working fluid.

Producing the geometry of the compressor stage brought up an idea about an analogy between pipe bend losses and impeller shape losses. This hypothesis was tested with a shrouded impeller that has only radial. This impeller type was common in the early days of centrifugal compressors. The analogy was found false.

1.1 Current state of refrigeration in aeroplanes

Most modern jetliners have need for refrigeration and air conditioning. They mostly rely on air cycle machines, see Figure 1.1.1. The air cycle machine takes the bleed flow from the gas turbine engine, which is above the ambient temperature, cools it down with atmospheric air, compresses it further, and then removes the heat from it again. Now the pressurised air, somewhat above the ambient temperature, is fed to an expansion turbine where it cools down and produces force to drive the compressor. The air at the outlet of the air cycle is considerably cooler than the atmospheric air. This exhaust air is then used for refrigeration.

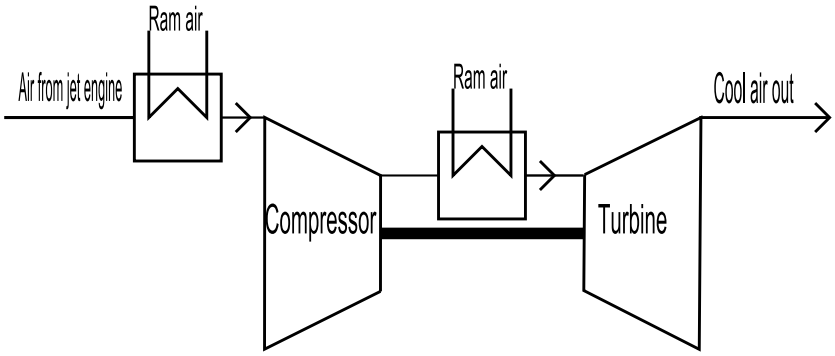

Figure 1.1.1: A simplified process layout of air cycle machine. The inlet pressure is considerably higher than outlet pressure, thus the turbine can power the compressor and no electric motor is needed.

Aircrafts need cooling at all stages of operation, but the most cooling power is needed on a hot day while the aircraft is on the ground with passengers onboard. But even during the flight at high altitudes there is need for to cool down the power electronics and in the galleys there is need for refrigeration for hygiene reasons. The ram air usage is restricted as it heavily

increases fuel consumption. Also the ram air is in lower pressure at high altitudes and can not be used directly for cooling inside the fuselage that needs to be pressurised. The above means that the off-design range of the thermodynamic cycle needs to be large and it is common to use several machines in parallel.

The air cycle system has many advantages for passenger aeroplane use, as presented by Wang and Yuan (2007). It is light and robust. Its lightness is due to high-speed technology. High rotational speeds in turbomachinery enables high power density and thus light weight. The prerequisite for high rotational speed are touch free bearings. Most air cycle machines use gas bearings, but in other high speed applications magnetic bearings are common. Touch free bearings also enable the machine to be oil free. Together touch free bearings and oil free machinery lead to higher reliability. As it is powered externally by the gas turbine engine it does not need to have an electric motor. Thus very high rotational speeds are available. Air cycle technology is well matured Furthermore, the working fluid is air, which is not harmful for health nor environment unlike many working fluids of vapour cycle machines.

However, the increasing concerns about global warming has led some aeroplane manufacturers to look for more energy efficient refrigeration. The air cycle has innate low efficiency when compared to vapour cycle, presented in Figure 1.1.2. Systems involving phase change need less compression work as the specific enthalpy of condensation and evaporation in condenser and evaporator rises the capability of fluid to release and capture energy per unit of mass. Also, the air cycle machine is powered by the motor or an auxiliary power unit, which are located at the wings and at the back of the aeroplane. The cooling power is needed in the fuselage. Thus there is need for piping, which increases the weight. It is also more efficient to produce the energy to drive refrigeration by an electric generator than by bleed flow. More over, modern jetliner employ high bypass ratio jet engines and leakage flow taken after the high pressure compressors reduces the thrust more, the higher the bypass ratio is.

1.2 Potential of vapour cooling systems

Vapour cooling has higher COP relative to single-phase cycles, particularly for low temperature differences between heat source and sink. The aircraft manufacturers however are not interested in the efficiency of the single components, but on the overall fuel consumption of the jetliners. The overall weight of the aeroplane is crucial for the fuel consumption, thus the light

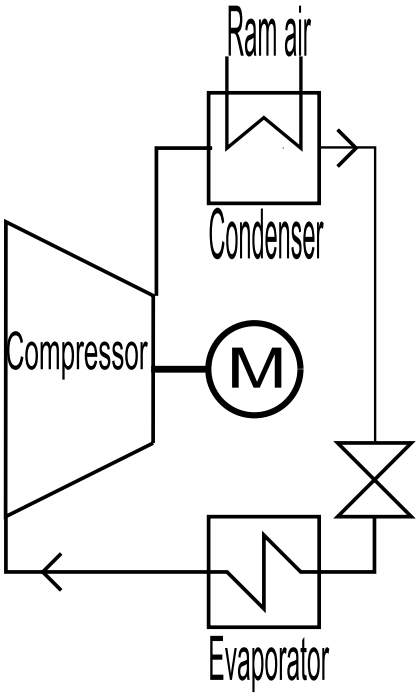

Figure 1.1.2: Principle of vapour cooling system. The compressor is powered by an electric motor. Evaporator absorbs heat thus cooling the environment.

weight of the machinery is of great importance. With a high-speed centrifugal compressor, the weight can be brought down to a competitive range when compared to the air cycle machine. This can mean that the overall fuel consumption with the vapour cooling cycle is lower than with the air cycle. The topic has been studied in the MOET project, but the results are still inconclusive.The energy consumed by the vapour cooling is certainly lower. However, as stated before the weight of the machinery also affects the overall energy efficiency.

Should the refrigeration be powered by electricity, there would certainly be more electricity consumed in aircraft than with air cycle machines, and this would lead to some changes in the power distribution and generation systems. The general trend in aeronautics is that modern aircrafts have less and less mechanically powered auxiliary systems.

It should be noted that reciprocating compressors are not considered because of their lower power-to-weight ratio. Reciprocating compressors also have lower isentropic efficiencies. Wilson (1988)

Another benefit of the vapour cooling system are the lighter heat exchangers. Because of the phase change in heat exchangers, the heat ex-

changers can be lighter than air-air heat exchangers.

The vapour cooling system prototype developed in this study is very light. As mentioned before the compressor converts electric energy to kinetic energy to operate. As it also utilises variable speed control and high rotational speeds it needs frequency converter to operate. Due to the large range at very high rotational speeds a filter for the electric current signal has to be employed to avoid excessive heating of the electric motor's stator due to the harmonic frequencies generated in the frequency converter. These electric devices are referred as power electronics. The standard power electronics used in the prototype were 10 times heavier than the compressor itself. Thus it would be necessary to reduce the weight of power electronics should this vapour cooling cycle technology be mounted on an aircraft.

The performance values reported for an optimised air cycle machine in the same power range are much poorer. (Spence et al., 2005). They can not even match the performance of a conventional vapour cooling cycle with a reciprocating compressor. It is fair to say that this process is superior to the air cycle in efficiency. Consequently, it needs less energy to operate and thus contributes less to the climate change, especially when compared to the actual machinery built by Spence et al. (2004).

1.3 Research goals

This thesis presents a part of the investigations realised within the the frame of the MOET project, a FP 6 european integrated project. The goal of the sub work package realised by the fluid dynamics research group of Lappeenranta university of technology in collaboration with Liebherr Aerospace Toulouse was to develop a high efficiency light-weight vapour cooling system. This should be done within the safety and environmental requirements set by the aerospace industry. It was not within the framework of this study to compare the different cooling cycles. The sole purpose was to provide a prototype for the vapour cooling system and to demonstrate its capacity.

The rather small cooling power presents challenges for the aerodynamic design, even more so than in air cycle machines. In vapour cycle the specific cooling power is high and thus the volumetric flows are small. This naturally requires small impellers, leading to a low Reynolds number and relatively large boundary layers in the impeller. Because of the high rotational speed, touch-free bearings are needed. Touch-free bearings have in general large clearances when compared to ball bearings and the high power density of the machine causes high temperatures of the rotor leading to thermal expansion further increasing clearance. This causes performance deterioration from

the values usually achieved with centrifugal compressors. In this work, it is demonstrated that despite the technical difficulties the centrifugal compressor still performs rather well.

The most important goal illustrated in this thesis is the development of the special design needed to successfully realise a vapour cooling system of this size range. The design procedure and the anticipated results are presented in the study. The results obtained from the actual vapour cooling system prototype are not within the scope of this thesis.

Chapter 2

Screening of working fluids

2.1 Introduction

The most important decision in design of an air-conditioning system is the working fluid selection. Modern high-speed technology makes it possible for the refrigeration compressor to be completely oil free, which considerably broadens the scale of possible working fluids as oil solubility demands can be relaxed. Furthermore, many traditional fluids have become banned and the industry standard R134a might face the same fate in some European countries because of its relatively high global warming potential.

The air-conditioning system fluid is selected for is a prototype of vapour cooling system for a jetliner. As always efficiency is important, but in this particular application weight is also of great importance as explained in the previous chapter. Environmental effects of the working fluid are also considered. Flammable and toxic fluids can not be employed.

In this study eleven different fluids were studied and compared and R22 was used as a reference, as it is the old industry standard fluid for centrifugal chillers. It was found that there are potential fluids for centrifugal compressors that provide better efficiencies than the most common fluid, R134a, in use today. The purpose of this study is to screen fluids for closer inspection.

The fluids are evaluated by the efficiency of the cycle, but also mechanical feasibility and dimensions are considered as light weight of the machinery is an important criterion in design process. Some properties of the fluid lead to unwanted mechanical features, e.g. low density at the inlet of the compressor leads to large impellers as the same amount of power is required. Besides increased weight, large impellers lead to high peripheral speeds causing high stress levels that make mechanical design difficult if not impossible. Another unwanted property is extremely low pressure at the evaporator, as it would

make preventing air leakage into the system difficult. This does not mean that subatmospheric pressures make the system unfeasible, this is only the case when the pressures are very low i.e. less than approximately 20 kPa.

The comparisons is based on the evaluation of the performance of systems implementing the thermodynamic cycle of Fig. 2.1(b), at fixed evaporation and condensation temperature presented in table 2.3.2. The cooling capacity of the system was fixed, but the actual value of the capacity cannot be revealed due to the wishes of the customer. It can be stated that it is much lower than usual values with centrifugal compressors, clearly under 30 kW. The isentropic efficiency was determined based on the semi empirical curves of isentropic efficiency against specific speeds presented by Balje (1981). The safety factors often play a dominant role and were also shortly considered.

Similar study for idealised compression cycle was performed by Brown (2007). However for centrifugal compressor the isentropic efficiency varies with fluid properties as do the dimensions of the stage, so the results and the method presented are not directly applicable.

We chose to use a high speed compressor with a permanent magnet motor and a frequency converter. This enables high rotational speeds with good efficiency (Arkkio et al., 2005).

Previously centrifugal compressor performance has been modelled by Browne and Bansal (1998) and Bein and Lee (1999). At this part of the study we resorted to somewhat simplistic model of centrifugal compressor as this is only initial screening.

It is well established that the most important adverse environmental effect of refrigeration is the CO_2-emissions from the production of electric energy converted to the kinetic energy of the compressor by the system. (Calm, 2002). In article by Calm (2006) the actual global warming, including energy consumption, caused by the fluid used in refrigeration was studied.

This work is done to present the possibility of evaluating working fluids for given temperature and cooling power with relatively light computational method. The calculations required can be done on any modern desk top PC within seconds. This model contains many simplifications and a more complete and laborious method was later developed (Röyttä et al., 2009).

2.2 Method

2.3 Process Description

The comparison process is greatly simplified from the actual process. Pressure losses in pipings and heat exchangers were modelled with relative pres-

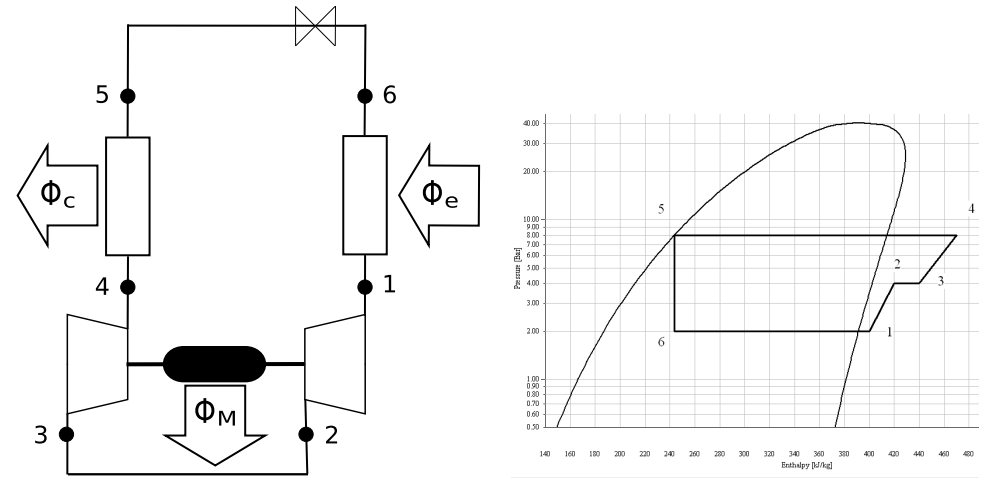

(a) (b)

Figure 2.3.1: Principle of the process. In outlay (a) the low pressure compressor on the right side. The thermal principle in (b) is presented in log p, h chart.

sure drops.

The process used in comparison consists of a two-stage centrifugal compressor, with permanent magnet electric motor cooled with the working fluid, see Fig. 2.1(a). There is no intercooling. The heat generation of the electric motor varies as a function of the electric power and rotational speed. The process flow diagram of the vapor-compression system and the corresponding process in the P-h thermodynamic plane are presented in Figure 2.1(b).

The heat removed from the environment is absorbed into the refrigerant in the evaporator where the vaporizing temperature is lower than that of the environment. The refrigerant is vaporized and superheated in the evaporator. The low pressure (LP) compressor compresses the gaseous refrigerant to the intermediate pressure between the compressors, which is one of the optimisation variables. The gaseous refrigerant flows from the LP compressor through the electric motor to the high pressure (HP) compressor that compresses the gas to the condensing pressure. The isentropic efficiency of the compression process is determined based on the specific speed of the impeller. The heat from the process is transferred to the environment in the condenser where the refrigerant is first desuperheated, and then condensed into a liquid. The condensing temperature is higher than that of the environment. The liquid refrigerant returns to the evaporator through the expansion valve where the liquid expands to the evaporator pressure in an isenthalpic process and un-

Table 2.3.1: Fluids used in comparison

Shorthand	Explanation	GWP	Flammable	Toxic
R22	Chlorodifluoromethane	1700	No	No
R134a	1,1,1,2-tetrafluoroethane	1300	No	No
R290	Propane	20	Yes	No
R407c	R32/R125/R134a 23%/25%/52%	1700	No	No
R410a	R32/R125 50%/50%	2000	No	No
PFP	Perfluoropentane	7500	No	No
R601a	Isopentane	11	Yes	Yes
R600a	Isobutane	20	Yes	No
R245fa	1,1,1,3,3-pentafluoropropane	950	No	No
HFE-7100	Hydrofluoroether	297	No	No
R718	Water	0	No	No
R717	Ammonia	<1	No	Yes

dergoes cooling and partial vaporising. Thus, the refrigerant entering the evaporator is a mixture of liquid and vapor. More accurate description of the model can be found from Appendix I and from Kuosa et al. (1998).

2.3.1 Fluids Used in Comparison

In this comparison we chose fluids that are interesting and ones that have been found feasible for vapour cooling systems utilising centrifugal compressors in the past. The fluids are listed in Table 2.3.1. Carbon dioxide was not studied due to its high evaporating and condensing pressure, which would lead to heavy piping. Should the same study be done for a system of which weight is not critical it would be an interesting fluid. The GWP values presented here are from (Calm and Hourahan, 2001), except HFE-7100 and PFP, which are from (Solomon and Qin, 2007).

2.3.2 Fluid properties modelling

The computer code used in the calculations utilises an old computationally fast model for fluid properties. The model for thermodynamic properties is documented by Talonpoika (1994). The calculation of dynamic viscosity

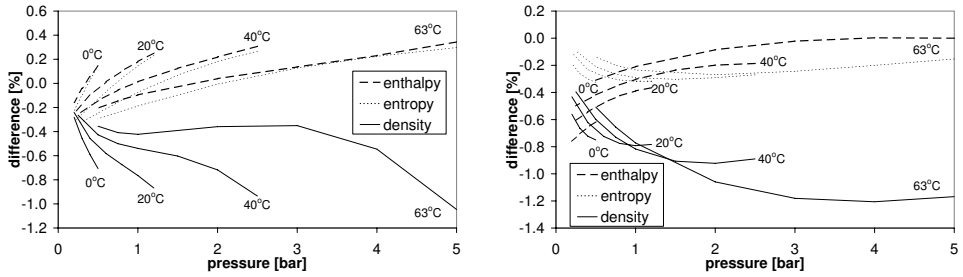

(a) (b)

Figure 2.3.2: The difference in thermodynamic properties between the model used and Refprop 8.0 for (a) R245fa and (b) R134a.

is based on the theory presented by Lucas (1988). Viscosity is not used for the thermodynamic modelling, but for the corrections of the isentropic efficiency of the compressor stages. These property models also enable the addition of a new working fluid by giving the input values, generally available in tables, without having to program a new calculation routine. The main reason to choose this model was that it was readily implemented in the code and that as the in-house program was made with turbo-pascal programming language the interface between REFPROP and the code would have been time consuming to realise.

The models were compared to REFPROP 8.0 (Lemmon et al., 2007). REFPROP is considered as the state of the art of fluid property modelling. The results for thermodynamic properties of R245fa and R134a are presented in Fig. 2.2(a) and 2.2(b). The dynamic viscosity predicted by the model and that taken from REFPROP 8.0 for the same fluids are compared in Fig 2.3(a) and 2.3(b), respectively. It can be seen that the thermodynamic properties are accurate, but the dynamic viscosity has deviation from the values predicted by REFPROP up to 10 %. This error mainly affects the correction factors of the efficiency.

2.3.3 Comparison criteria

The power consumption is the most important criteria for the evaluation of successful design. In a jetliner the power consumption of a vapour cooling system comprises of two elements, the power consumed by the system and the additional power need of jet engine because of the weight addition caused by the system. The measure of the efficiency of the system is the coefficient

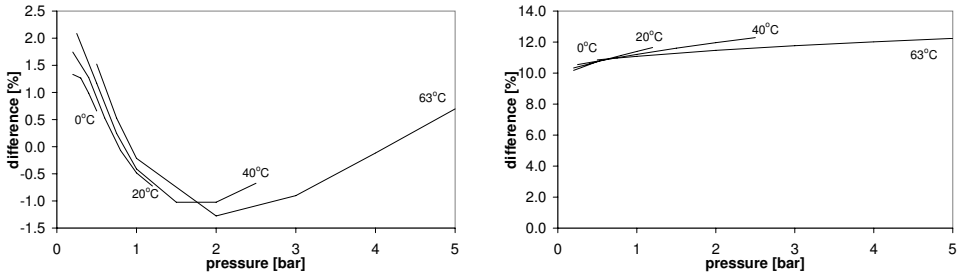

(a) (b)

Figure 2.3.3: The difference in dynamic viscosity between the model used and Refprop 8.0 for (a) R245fa and (b) R134a.

of performance (COP)

$$\mathrm{COP} = \frac{\phi_{\mathrm{cool}}}{\dot{W}_{\mathrm{el}}} \tag{2.3.1}$$

The optimisation for this case, however is done to maximise the thermal Coefficient of Power. COP calculated from eq. 2.3.1 takes into account the isentropic efficiencies of the compressor stages, as well as the mechanical and electrical losses of the whole compressor unit. In eq. 2.3.2 COP_{th} based on thermal power $\dot{W}_{\mathrm{th}}$ considers only the isentropic efficiencies of the compressor stages.

$$COP_{\mathrm{th}} = \frac{\phi_{\mathrm{cool}}}{\dot{W}_{\mathrm{th}}} \tag{2.3.2}$$

Another important comparison criteria is relative Mach number at the impeller tip. The Mach number is evaluated at the impeller blade leading edge tip, where the relative speed is highest. Combinations of intermediate pressure and rotational speeds leading to The subsonic velocities are preferred because the supersonic velocities produce extra losses.

$$M = \frac{V_{\mathrm{le,tip}}}{a} \tag{2.3.3}$$

The COP of the refrigeration cycle is determined based on the values presented in Table 2.3.2. The COP of R718, water, was calculated with higher evaporation temperature because the triple point of water is higher than $0°C$. As the COP of the system is in general better the smaller the temperature

Table 2.3.2: Initial values for calculations

Evaporation temperature	$0°C$
Evaporation temperature for R718, water	$5°C$
Condensation temperature	$40°C$
Superheating at evaporator	$5°C$

difference between condensation and evaporation, this is justified only if the COP of R718 is considerably weaker than that of the best fluids. In our experience on previous designs the change in condensation temperature usually leads to quite similar changes in COP between fluids, but the changes in evaporation temperature and cooling power easily change the superiority of fluids. An additional input for the calculations was the cooling capacity but as stated before, it can't be disclosed.

The performance of the compressor was modelled with in-house computer code. The details are presented in a separate subsection. The purpose of the code is not to make accurate design but to estimate the overall efficiency the fluid provides for the given system. The code is further developed from the one presented by Kuosa (1994).

2.4 Results

The results presented in Table 2.4.1 were calculated with an in-house computer code. The results show that there are many fluids that provide significantly higher COPs than the most widely used R134a yields, see Figure 2.4.1. The big differences between thermal COPs and total COPs are explained by the gas friction losses in motor cooling.

It should be noted that the rotational speed and intermediate pressure are optimised to get the best possible thermal efficiency in the compression process. This leads to higher rotational speeds and friction losses than optimising with respect to the overall efficiency. The final optimisation of the system is done considering the overall efficiency. Current state of the permanent magnet motors and inverters allow speeds up to 110 000 Arkkio et al. (2005). However, as the final design would certainly have lower rotational speeds than estimated here, it can be concluded, that those fluids that would require rotational speed of over 150 000 are not feasible.

As the manufacturing cost and safety are of great importance the fluids

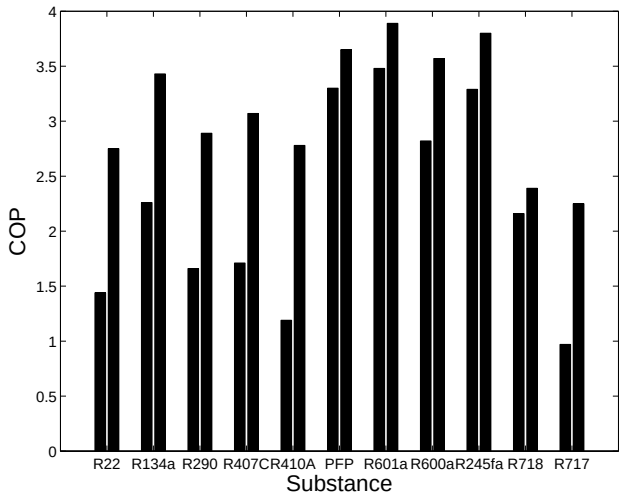

Figure 2.4.1: Cop values of different substances, Taller bars are thermal COP, shorter COP values

with very low evaporating pressure or high condensation pressure should also be discarded. The sub-atmospheric pressure is not an issue, but e.g. in Table 2.4.1 the evaporation pressure of HFE-7100 is 8.5 kPa, which is certainly too low as it would set too high requirements for the hermeticity of the evaporator.

For the specific application of this project, flammable fluids were excluded, but otherwise hydrocarbons would offer really attractive choices.

All substances with ozone depletion potential (ODP) have long been banned, thus R22 doesn't come in to question. However as can be seen, it wouldn't be an ideal solution for this application.

In this particular case the desired GWP value of the fluid was that of R134a or lower. This excludes PFP, that otherwise would have been an interesting candidate.

The constraints of this project leave us finally with two considerable fluids, R134a and R245fa. The choice between them culminates to the choice whether the sub-atmospheric pressures are tolerated. With modern technology it is relatively easy to make a hermetic compressor, thus R245fa with higher efficiency and more reasonable rotational speed was chosen.

Table 2.4.1: Overall results, more results are presented in Appendix I.

	COP	COP_{th}	Rotational speed krpm	Inlet pressure kPa	Outlet pressure kPa
R22	1.44	2.75	166	494.2	1725.5
R134a	2.26	3.43	131	290.5	1151.5
R290	1.66	2.89	240	473.6	1519.8
R407c	1.71	3.07	154	450.0	1718.3
R410a	1.19	2.78	1874	794.3	2689.7
PFP	3.30	3.65	31	29.6	174.7
R601a	3.48	3.89	93	34.0	175.6
R600a	2.82	3.57	160	153.4	589.4
R245fa	3.29	3.80	76	53.2	294.4
HFE-7100	3.25	3.52	23	8.5	60.2
R718	2.16	2.39	112	1.1	10.3
R717	0.97	2.25	676	438.3	1777.2

Chapter 3

Selection of the optimal design parameters for the system

3.1 Introduction

The final system composition, two stage centrifugal compressor with a flash intercooler was decided by the customer with some input from LUT. The temperature levels required determine the overall pressure ratio. In this part of study the system performance was simulated with two working fluids, R245fa and R134a.

The centrifugal compressor provides better efficiency wit a wide operational range (Dixon, 1989) and better power-to-volume ratio (Wilson, 1988), if compared to a displacement compressor. Thus, they should be adopted in refrigeration systems, if possible, whenever low power consumption and weight are desired. The performance of the centrifugal compressor has a strong dependence on the working fluid and the operational range(Brown, 2007; Calm, 2006). The main parameters dictating the centrifugal compressor efficiency are specific speed, specific diameter. Reynolds number limits the efficiency in small size compressors. The density of the gas is the most important property in these figures, it has to fall in the right range. However the density of the gas and the mass flow are not alone enough to predict the performance.

In an article by Brown (2007), the efficiencies of refrigerants for idealised vapour cooling cycle based on the properties from REFPROP 8.0 were studied and compared to a model requiring less data by Saleh and Wendland (2006). In our study a more machine-specific approach is required. Theoretical studies concerning the COP of the idealised vapour cooling systems are numerous, e.g. (Ust and Sahin, 2007; Chen et al., 2002; d'Accadia and

de Rossi, 1998). A summary of steady-state vapour compression cycle modelling has been presented recently by Guo-liang (2007). A somewhat similar summary has been done by Winkler et al. (2008). Vaidyaraman and Maranas (1999)wrote an interesting article concerning the optimisation of the refrigeration system configuration with the possibility to use different fluids.

Browne and Bansal (1998) have also carried out a similar study concerning the efficiency of a centrifugal compressor. The article presents an investigation about a one-stage compressor refrigeration system that operates at low speeds using R11 as a refrigerant. In our study, the weight of the cycle is also essential and therefore small heat exchangers were selected. This leads to a higher condensation temperature as well as a rather high pressure ratio for these fluids. The overall pressure ratio is in order of 10, in helicopter gas turbine engines pressure ratios of 6 can be achieved with single stage, but this high pressure ratios lead always to transonic design and thus lower efficiencies especially at off-design conditions. Therefore, it is clear that a one-stage compressor is infeasible.

When selecting the working fluid, a non-flammable fluid with a relatively low global warming potential (GWP) and zero ozone depletion potential (ODP) is required. Many hydrocarbons that would have offered environmentally sustainable, high efficiency options (Saleh and Wendland, 2006) were discarded by the customer as possible working fluids because of their flammability. Other natural refrigerants were also considered, but were not particularly favourable, e.g. CO2 would have very high pressure levels and thus very heavy heat exchanger and piping and for this cooling capacity the impeller size or to be exact, the Reynolds number in impeller passage is too small. Very low sub-atmospheric pressures, e.g. water, would also lead to very heavy machinery. This is due to two reasons, mechanical strength required in the evaporator leading to large material thickness and the large volumetric flow leading to large volume of the components.

R134a and R245fa were eventually selected, the former being the most widely used fluid in todays centrifugal chillers. The fluids have GWP of 1320 and 1020 respectively Calm (2006). The GWP values are determined for the 100 year time horizon. Both values can be considered high and it is possible that because of this they will be banned in European union.

3.2 Methods

The objective of this study is to determine the optimal working conditions for the refrigeration system described below. We choose to compare R134a and R245fa partly because we want to check the results of the screening and

as we want to be certain of the benefits of R245fa before deserting industry standard R134a.

The calculation of the refrigeration process begins by determining the mass flow through the evaporator. This mass flow is defined using the required cooling power:

$$q_{m,eva} = \frac{\dot{W}_{cool}}{h_{13} - h_{11}} \tag{3.2.1}$$

The refrigerant is a real gas and the enthalpy is defined as a function of pressure and temperature. The temperature before the evaporator T_{11} is given and the evaporation pressure is calculated. However, the process point 11 will be in the wet vapour area, and the vapour content is needed to define the enthalpy. The vapour content is determined as follows:

$$x = \frac{h - h_{\mathrm{l}}}{h_{\mathrm{g}} - h_{\mathrm{l}}} \tag{3.2.2}$$

The vapour content is calculated after the cooling process, and therefore it must be presented as an initial estimate. The pressure drop and the degree of superheating in the evaporator are initial values, see table 3.3.1. Now the enthalpy after the evaporator, h_{13}, can be calculated. The calculation of the evaporator is defined in section 3.2.2. The pressure before the compressor's first stage is determined by:

$$p_1 = p_{13} - \Delta p_{13} \tag{3.2.3}$$

where the pressure loss Δp_{11} is a given value and depends on the piping. The enthalpy before the compressor's first stage h_1 is determined by using the enthalpy and mass flows coming from the evaporator, h_{14} and q_{m14}. To determine the fluid state after the compressor stage the isentropic enthalpy change is calculated. This is possible as the intermediate pressure is a optimisation variable. Then, as the mass flow is calculated from the cooling capacity the specific speed of the compressor stage is given and rotational speed is optimisation variable the specific speed can be calculated from equation 3.2.4. Specific speed is then used to calculate the isentropic efficiency, see Figure 3.2.2 and then corrections to the efficiency are applied. With the isentropic efficiency the actual enthalpy change over the compressor can be calculated. The cooling of the electric motor is done with the refrigerant. The pressure drop in the electric motor is given and the calculation of the heat from the electric motor is defined in section 3.2.3. The state before the compressor's second stage (4) is calculated combining the flows coming from

the electric motor and the flash intercooler. The compression in the second stage is calculated similarly as the first stage. The outlet pressure is now determined by the condenser temperature T_6. The calculation of the condenser is defined in section 3.2.2. The mass flow going through the flash intercooler is calculated from the energy balance. The temperature after the intercooler T_{10} is defined to be $5°C$ superheated and it is calculated using the pressure before the second stage. The pressure drop due to the piping is taken into account. The pressure drops in the valves are assumed isenthalpic.

The working fluid was similarly modelled as in section 2.3.2.

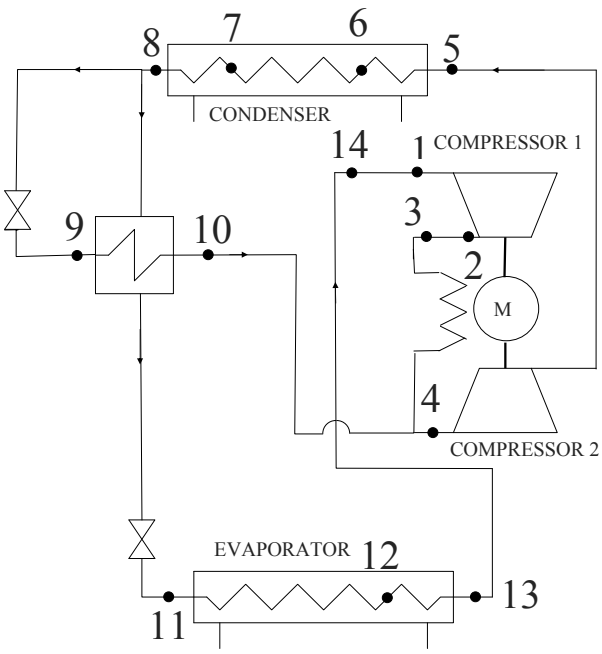

Figure 3.2.1: Flow chart of refrigeration process.

3.2.1 Compressor model

The operation of the compressors have been modelled using the semi-empirical model, which utilises the specific speed of the compressor to determine the isentropic efficiency, see Fig. 3.2.2. The corrections to this efficiency are made by taking into account the Reynolds number, relative surface rough-

ness and the relative blade tip clearance. The specific speed of the compressor is determined by:

$$N_s = \frac{\omega\sqrt{q_{v1}}}{\Delta h_s{}^{0.75}} \tag{3.2.4}$$

where ω is the angular speed of the impeller and subsequently shaft's, q_{v1} is the volume flow at the compressor inlet and Δh_s is the isentropic enthalpy change over the compressor.

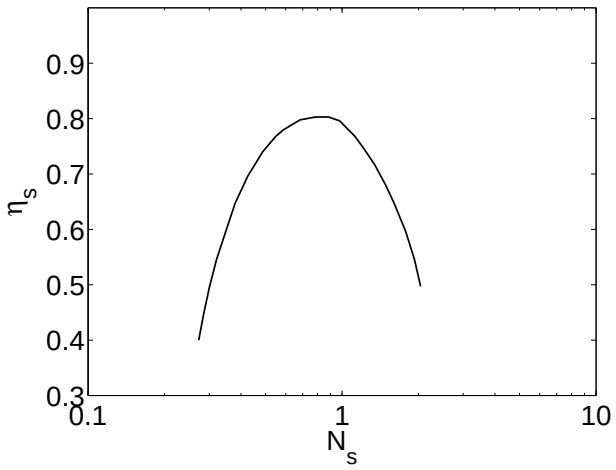

Figure 3.2.2: Isentropic efficiency as a function of specific speed. The data is from an article by Balje (1962)

The Reynolds number correction is made according to Casey (1985). The Reynolds number is calculated using the blade height at the rotor outlet as a reference measure

$$Re_b = \frac{\rho \cdot U \cdot b}{\mu} \tag{3.2.5}$$

where $U = 2 \cdot \pi \cdot r$ is the peripheral velocity of the impeller trailing edge, b is the blade height and μ is the dynamic viscosity of the fluid. To calculate the Reynolds number, the dimensions of the compressor wheel are needed, and they are estimated using the compressor's loading coefficient.

$$\psi = \frac{\Delta h}{U^2} \tag{3.2.6}$$

It is assumed that the loading coefficient is 0.6, which is a common design value. This is necessary to find a value for the peripheral velocity. The blade height is estimated using the data from several prototypes manufactured in Laboratory of Fluid Dynamics, LUT.

The effect of the relative surface roughness of the flow channel is taken into account by correcting the Reynolds number. This method takes in account the performance deterioration caused by surface roughness by calculation of a virtual corrected Reynolds number. The Moody chart (Kast, 1988) is useful in illustrating the method of correcting the Reynolds number, because it gives the friction coefficient as a function of the Reynolds number and the relative surface roughness. The main principle is to take in account increased losses caused by increased surface roughness. The article by Casey (1985) gives the efficiency penalty of decreasing Reynolds number. In that article the relative surface roughness is given. In our correction method first the friction factor with the actual relative surface roughness and Reynolds number is calculated from *Colebrook-White* equation Kast (1988)

$$\frac{1}{\sqrt{\xi}} = -2\lg\left[\frac{2.51}{Re\sqrt{\xi}} + \frac{K_{\text{rel}}}{3.71}\right]. \tag{3.2.7}$$

Where Re is the Reynolds number and K_{rel} is the relative surface roughness. Then the corrected Reynolds number is calculated by solving the equation 5.1.3 for Reynolds number and solving it replacing the relative surface roughness of the case by the reference value from Casey's article and by placing the friction factor calculated into the equation. Then this corrected Reynolds number is used with the correlation from Casey (1985) to calculate the efficiency change.

The relative blade tip clearance at the trailing edge is inversely proportional to the efficiency of the stage at feasible range. See Musgrave (1980) for correlation.

3.2.2 Heat exchanger model

The heat exchangers in the process i.e. the evaporator and the condenser, are treated using different zones. The evaporator is divided into two zones, a two-phase and a superheated vapour zone, and the condenser into three zones, a superheated, a two-phase and a subcooled zone. The pressure drops in the heat exchangers are defined as a percentage of the total pressure, and they are divided into each zone such that 1/8 of the pressure drop takes place in either the superheated or subcooled zone. There is no energy flux to, or from the flash intercooler, and it operates in steady state.

3.2.3 Electric motor calculation

Here the electric motor losses are chosen to be scaled from values of previous designs, measured as part of the studies documented in Ph. D. dissertation

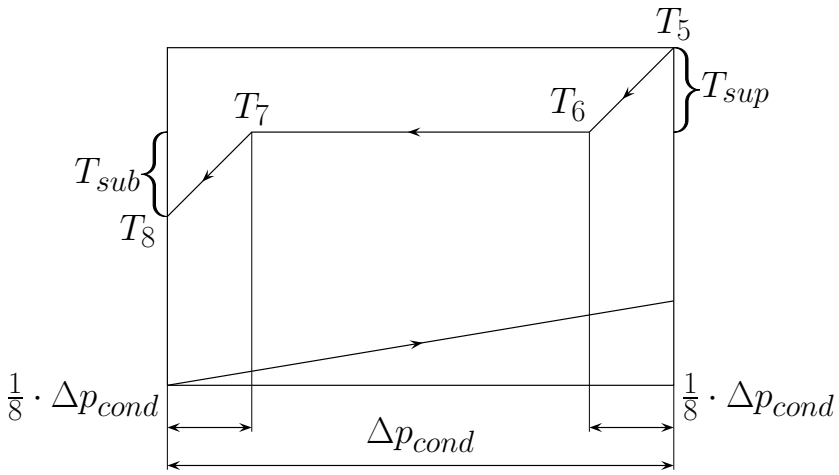

Figure 3.2.3: Changes in pressure and temperature in the condenser.

of Saari (1998). This is a simple way to get a good estimation. The scaling is based on the assumption that the electric motor dimensions vary in respect to it's peak power. The scaling presented here was developed in Röyttä et al. (2009), Appendix II.

The mechanical losses in the air gap comprise two elements: the friction loss and the power needed to accelerate the fluid to the tangential velocity (Saari, 1998)

$$P_{\mathrm{ec}} = P_{\mathrm{gf}} + P_{\mathrm{af}}. \tag{3.2.8}$$

The friction loss is

$$P_{\mathrm{gf}} = k_1 C_{\mathrm{f}} \rho \pi \omega^3 r_{\mathrm{r}}^4 l. \tag{3.2.9}$$

where k_1 is the roughness coefficient and C_{f} is the friction coefficient.

Then the proportionality of P_{gf} to r_{r} is

$$P_{\mathrm{gf}} \propto \rho^{1.2} r_{\mathrm{r}}^{4.8} \omega^{3.2} \mu^{0.2} \tag{3.2.10}$$

as we assume that the shape of the electric machine remains constant as it is scaled down. Thus, δ / r_{r} is constant.

A equation for the losses associated with accelerating the fluid to tangential velocity is Saari (1998)

$$P_{\mathrm{af}} = k_2 q_m \left(\omega r_r\right)^2. \tag{3.2.11}$$

The axial flow losses have the following dependencies

$$P_{\mathrm{af}} \propto q_m \left(\omega r_{\mathrm{r}}\right)^2 \tag{3.2.12}$$

The reference values were taken from the measurements done previously in the Laboratory of Fluid Dynamics, LUT, documnted in Saari (1998). The articles written by Kuosa et al. (2004, 2005) could be used as an alternative source.

3.2.4 Optimisation model

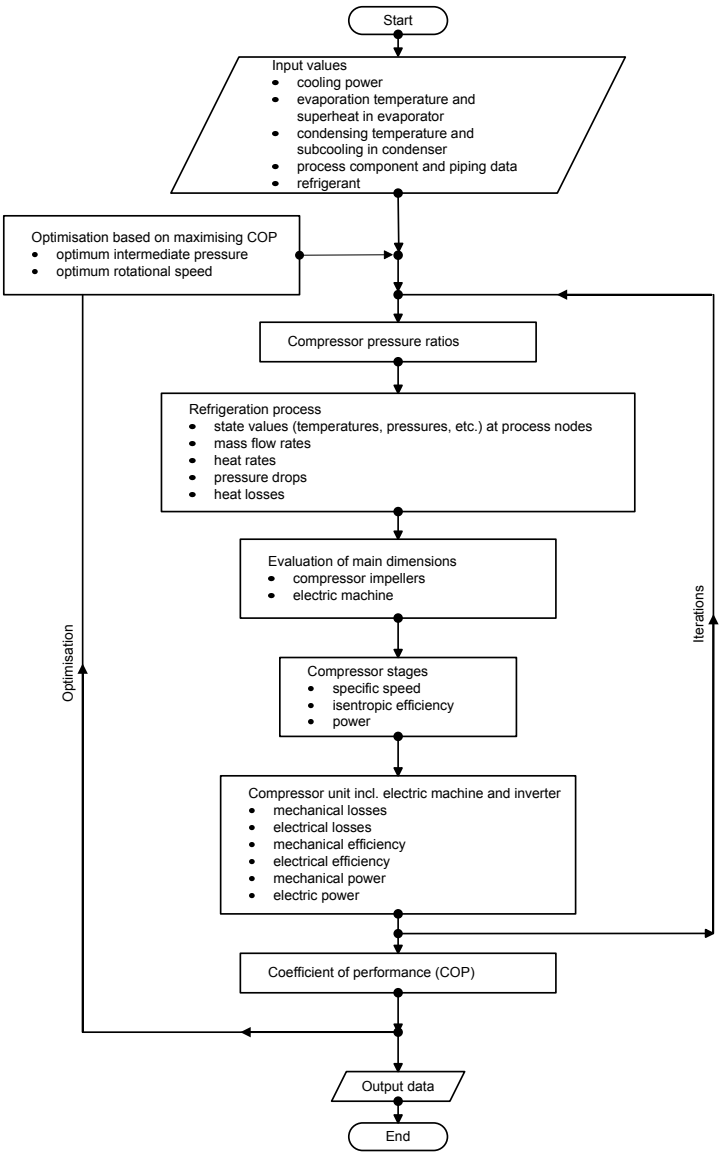

Figure 3.2.4: Optimisation and calculation procedure

The refrigeration process is optimised by maximising the coefficient of the performance (COP). The COP is determined by

$$COP = \frac{\phi_{\text{cool}}}{\dot{W}_e} \tag{3.2.13}$$

where ϕ_{cool} is the required cooling power and $\dot{W}_e$ is the electrical power. The electrical power is calculated by

$$\dot{W}_e = \frac{(\dot{W}_{c1} + \dot{W}_{c2} + \dot{W}_{bearing} + \dot{W}_{ec})}{\eta_e} \tag{3.2.14}$$

where η_e is electric motor and inverter efficiency, $\dot{W}_{c1}$ and $\dot{W}_{c2}$ represent the power of each stage, $\dot{W}_{bearing}$ is the bearing friction power, and $\dot{W}_{ec}$ is the power consumed by mechanical losses in the air gap.

The calculation procedures are presented in Fig. 3.2.4. Calculation of the refrigeration process and the compressor unit is iterative containing several iteration loops within each other (not shown in detail in Fig. 3.2.4). Firstly, the input values are given and the some inital guesses are made for recursive equations e.g. equation 5.1.3. The iterations are repeated until the given convergence conditions are satisfied. This procedure is performed each time in the optimisation loop.

3.3 Results

3.3.1 Initial values of the process.

The initial values of the refrigeration process are illustrated in Table 3.3.1. The cooling power, condensing temperature, evaporating temperature, bearing power loss, superheating in the evaporator and superheating after the flash intercooler are given. Two different refrigerants are modelled.

Table 3.3.1: Initial values of the refrigeration process.

T_c	$63°C$
T_e	$0°C$
$P_{bearing}$	$\frac{1}{20}P_{cool}$
T_{flash}	$5°C$

3.3.2 Overall performance of the refrigeration process

The overall performance of the refrigeration process was evaluated using the COP value. Optimisation was performed by changing the rotational speed and the intermediate pressure of the compressor. The performance values are confidential and had to be nondimensionalised. The best performance was achieved at the rotational speed of N_{opt} and at an 1$^{\text{st}}$ stage pressure ratio of $\pi_{c1,opt}$ with R245fa and at a rotational speed of $1.36N_{\text{opt}}$ and at an 1$^{\text{st}}$ stage pressure ratio of $0.67\pi_{c1,opt}$ with R134a, respectively. The COP value are higher with R245fa than values for the performance of R134a. The COP values were COP_{opt} and $0.77\text{COP}_{\text{opt}}$ for systems operating with R245fa and R134a, respectively. The values for the performance of the refrigeration process are presented in Fig.3.3.1 a for R245fa and in Fig.3.3.1 b for R134a. The best COP was achieved at a rotational speed of around N_{opt} at all intermediate pressures for R245fa. However, the optimum rotational speed is slightly lower with the higher intermediate pressure and vice versa. The optimum rotational speed differs at the different intermediate pressures for R134a. The same phenomenon is still visible -the optimum rotational speed is lower if the intermediate pressure is higher.

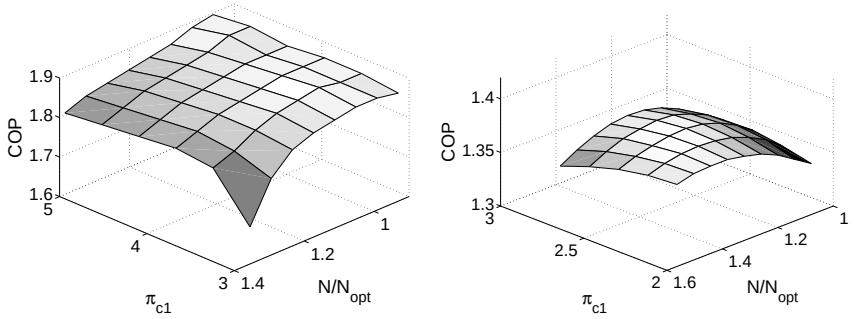

(a) (b)

Figure 3.3.1: COP with different rotational speeds and intermediate pressures with R245fa (a) and R134a (b)

3.3.3 Compressor performance

The two-stage compressor operation depends on the performance of both stages. In this process simulation, evaluation of the isentropic efficiency of the compressor is based on the specific speed, Reynolds number, surface roughness and relative tip clearance (see section 3.2.1). The pressure ratio, which determines the isentropic enthalpy change, and the rotational speed

affect the specific speed of the compressor stage (Eq. 3.2.4). Because both wheels are on the same shaft, an optimum specific speed cannot be selected for both compressor stages. Therefore, the pressure ratio and rotational speed need to be optimised in a way that both compressor stages achieve reasonable efficiency leading to the best possible overall compressor efficiency.

The variables in tables 3.3.7, 3.3.4, 3.3.6, 3.3.3 and **??** are made dimensionless by dividing them by the corresponding values at optimum point of the design. As the efficiency point is achieved with R245fa all the values, including those where the working fluid is R134a, are compared with that point.

The specific speeds, pressure ratio and isentropic efficiencies of both stages are presented in Tables 3.3.2 and 3.3.3 with R245fa. The stage efficiencies are made dimensionless by dividing them with the stage efficiencies at the optimum point of the process. The optimum COP point is presented and two points around it (corresponding changes in the rotational speed and intermediate pressure). The specific speed is higher with higher rotational speed. Because both wheels are on the same shaft, the optimum COP of the process is not achieved at the optimum specific speed of the either wheel. The isentropic efficiency of the first stage increases at the lower rotational speed but the isentropic efficiency of the second stage decreases.

The change in the intermediate pressure also affects the specific speed and consequently the isentropic efficiency as well. The specific speed in the first stage decreases while the intermediate pressure increases. This is due to the higher pressure ratio and therefore, higher isentropic enthalpy change. The specific speed in the second stage increases but the change is lower because the pressure ratio of the first stage is higher. Therefore, the inlet pressure of the second stage is higher, which leads to the higher density and lower volume flow to the second stage. In the light of the specific speed and isentropic efficiencies in Table 3.3.3 the higher intermediate pressure would be beneficial. However, the higher pressure ratio of the first stage leads to the higher power consumption of the first stage. At the same time, the power consumption of the second stage does not decrease enough to reduce the COP value. The power of the compressor stages, as well as the mechanical and the electrical power of the whole compressor are shown in Table 3.3.4 with R245fa.

The same performance parameters of the compressor stages are presented in Tables 3.3.5 and 3.3.6 with R134a as was previously presented with R245fa. The same trends are seen with R134a as is seen with R245fa. The magnitude of the specific speed of stages is lower than with R245fa and therefore the predicted isentropic efficiencies are lower. Lower specific speed is due to the higher density of the fluid. The pressure ratio of the second stage is higher

Table 3.3.2: Performance parameters as a function of rotational speed. Refrigerant R245fa and intermediate pressure 1st stage pressure ratio is $\pi_{c1,opt}$.

Rotational speed	$N_{s,c1}$	$N_{s,c2}$	π_{c1}	π_{c2}	$\eta_{s,c1}$	$\eta_{s,c2}$
0.94	0.829	0.504	3.39	3.23	1.00	0.98
1	0.883	0.536	3.39	3.23	1.00	1.00
1.06	0.936	0.569	3.39	3.23	1.00	1.01

Table 3.3.3: Performance parameters as function of intermediate pressure. Refrigerant R245fa and rotational speed N_{opt}.

π_{c1}	$N_{s,c1}$	π_{c2}	$N_{s,c2}$	$\eta_{s,c1}$	$\eta_{s,c2}$
2.97	0.954	3.70	0.528	0.99	1.00
2.39	0.883	3.23	0.536	1.00	1.00
3.81	0.831	2.86	0.548	1.00	1.00

Table 3.3.4: Power of compressor stages and mechanical and electrical power of whole compressor. Refrigerant R245fa.

rotational speed	$P_{c,c1}$	$P_{c,c2}$	P_m	P_e
0.94	0.200	0.236	0.514	0.551
1.00	0.200	0.233	0.513	0.550
1.06	0.201	0.230	0.513	0.551
π_{c1}	$P_{c,c1}$	$P_{c,c2}$	P_m	P_e
2.97	0.177	0.259	0.514	0.552
2.39	0.200	0.233	0.513	0.550
3.81	0.223	0.209	0.514	0.551

with R134a, and with R245fa the first stage pressure ratio is higher. This also leads to a different type of power distribution between the stages with R134a as compared to R245fa. The power of the stages and the mechanical and the electrical power of the entire compressor are presented in Table 3.3.7.

Table 3.3.5: Performance parameters as a function of rotational speed. Refrigerant R134a and 1st stage pressure ratio is 0.673 $\pi_{c1,opt}$.

rotational speed	$N_{s,c1}$	$N_{s,c2}$	π_{c1}	π_{c2}	$\eta_{s,c1}$	$\eta_{s,c2}$
1.30	0.618	0.396	2.28	2.77	0.96	0.88
1.36	0.647	0.414	2.28	2.77	0.97	0.89
1.42	0.676	0.433	2.28	2.77	0.97	0.91

Table 3.3.6: Performance parameters as function of intermediate pressure. Refrigerant R134a and rotational speed 1.36 N_{opt}.

π_{c1}	$N_{s,c1}$	π_{c2}	$N_{s,c2}$	$\eta_{s,c1}$	$\eta_{s,c2}$
2.11	0.693	3.01	0.406	0.97	0.89
2.28	0.647	2.77	0.414	0.97	0.89
2.46	0.611	2.57	0.424	0.96	0.90

Table 3.3.7: Power of compressor stages and mechanical and electrical power of whole compressor. Refrigerant R134a.

rotational speed	$P_{c,c1}$	$P_{c,c2}$	P_m	P_e
1.30	0.180	0.308	0.671	0.720
1.36	0.179	0.302	0.670	0.719
1.42	0.179	0.298	0.670	0.719
π_{c1}	$P_{c,c1}$	$P_{c,c2}$	P_m	P_e
2.11	0.159	0.328	0.670	0.718
2.28	0.179	0.302	0.670	0.719
2.46	0.199	0.278	0.670	0.720

Chapter 4

Off-design performance of refrigeration system

4.1 Introduction

In this chapter a study of the vapour cooling system off-design range and performance is presented at steady state conditions. It is based on combining the compressor maps of both stages and the system model. As the the high speed technology involves frequency converter we have the possibility to use rotational speed control to obtain the best possible efficiency at off-design conditions. Naturally the cooling capacity and thus the mass flow is another variable along with the condensing temperature.

Based on the studies presented before R245fa was selected as the working fluid. The aerodynamic design of the compressor stages was done. The compressor was modelled with CFD and modifications on the design on the basis of CFD results were done. A custom efficiency drop in the performance maps provided by 1-D design and CFD results was introduced as it is generally known that CFD results over predict the efficiency of the compressor stage. The resulting compressor maps were used for the modelling of the complete vapour cooling system.

By controlling the rotational speed it is possible to match wide range of cooling capacities with continuous operation of the system. This saves the system from repeated start ups related with traditional on-off controlling of cooling power. This also enables more flexible control and comfortable operation.

The rotational speed control's advantages in refrigeration systems have been studied but there are not many studies of systems using centrifugal compressors. The rotational speed control of the scroll compressor used in a

cooling loop has been tested experimentally by Aprea et al. (2006) and Aprea et al. (2008). It was noticed that by varying the rotational speed of the compressor to match the cooling load required, the consumption of electricity was decreased compared to the energy consumption of the on-off controlled compressor. Cuevas and Lebrun (2009) have studied the operation of the scroll compressor at a different rotational speed. The efficiency of the scroll compressor was not influenced significantly by the rotational speed. However, internal leakages were increased at the low rotational speed because there was no lubrication, and this slightly lowered the efficiency of the compressor. Koury et al. (2001) have conducted numerical simulation of refrigeration system. The rotational speed of the displacement compressor was altered. The increase in the rotational speed of the compressor increased the mass flow through the compressor and increased superheating in the evaporator. This led to a lower COP value. An inverter-driven scroll compressor with liquid refrigerant injection has been measured by Cho et al. (2003). The rotational speed of the compressor and injection locations were altered. At a high rotational speed, the liquid injection showed improvement in the performance and reliability of the compressor.

The studies concerning refrigeration cycles equipped with centrifugal compressors are not numerous. The thermodynamic modelling of centrifugal chiller system has been studied by Gordon et al. (1995). The chiller performance curve was found to be linear when compared to the cooling rate, optimal efficiency was found at the design point. The thermodynamic model was simple, and the operation of the compressor was not discussed. Browne and Bansal (1998) have studied centrifugal liquid chillers and their control using a steady-state model. The capacity control of the refrigeration process is presented and compared to the measured values. The control is conducted by prerotation vanes which are adjusted using the temperature of a chilled water flow. These vanes control the refrigerant mass flow rate. It was not mentioned that the rotational speed of the compressor was altered.

Cooling systems are seldom designed for a fixed point operation. Thus, it is essential to predict the off-design performance. Centrifugal compressors behave differently than displacement compressors in off-design conditions. The pressure ratio of displacement compressors is rather insensitive to rotational speed and mass flow, whereas the pressure rise in a centrifugal compressor stage is more sensitive to changes in mass flow and rotational speed. In centrifugal compressors, the operational range has some restrictions. The mass flow can not be restricted below the compressor's surge limit. The surge should be avoided because it damages the compressor, and it should be taken into account in the control of the compressor. As presented for example in Saravanamuttoo et al. (2001), compressor performance characteristics can

be presented graphically by means of a dimensionless rotational speed, and efficiency curves plotted against an equivalent flow and pressure ratio. These curves constitute the performance maps for a certain compressor. These map with dimensionless variables can be used to calculate the actual performance with varying inlet vapour conditions at different speeds.

Based on compression process calculations, the main characteristics of the compressor are designed (1D design) and performance maps can be developed. This is done by using two different compressor design codes, the in-house code Centriflow and the commercial code Compal by Concepts-NREC, to make the design more accurate and reliable. Using these two codes together gives more reliable surge line and decreases the risk of unrealistic results as it is often easier to see illogical behaviour of the maps if there is grounds for comparisons. The off-design calculation of the process with a flash-intercooler is conducted using the compressor performance maps created. The simulation of the whole refrigeration process is done at several points taking care that neither compressor stage surges, and one combined performance map is generated for the refrigeration process in order to study the cooling capacity and the efficiency.

4.2 Methods

The off-design modelling was realised by further developing the code described in the previous chapter and Appendix II.

The process cycle is similar to the one presented in 3.2.1. The superheating of the fluid at point 10 is fixed to 5 K.

The compressor maps are used to evaluate the operational speeds and the isentropic efficiencies of the stages. As only a limited amount of specific speed and efficiency curves have been generated for the performance maps, interpolation algorithms based on the study by Münzberg and Kurzke (1977) are used. This method applies linear interpolation of efficiency and pressure ratio from the known point presented compressor maps.

The inputs of the model were produced by varying cooling power and then optimising the rotational speed. A more complete description of the system modelling is given in Appendix III.

4.2.1 Compressor map

The performance map can be used to calculate the compressor performance when the operation differs from the design point. The calculation of compressor performance from maps is based on the routines presented by Traupel

(1966).

To produce the dimensionless maps two dimensionless variables have to be introduced. First, the dimensionless rotational speed is

$$\Phi = \frac{\omega}{\omega^*}\sqrt{\frac{T_{t1}^*}{T_{t1}}}. \tag{4.2.1}$$

Secondly, the dimensionless mass flow is presented as

$$\chi = \frac{q_m}{q_m^*}\frac{p_{t1}^*}{p_{t1}}\sqrt{\frac{T_{t1}}{T_{t1}^*}}. \tag{4.2.2}$$

The ordinate of the dimensionless performance map is pressure ratio π, the abscissa is χ from equation 4.2.2. The operational range is presented with dimensionless speed (equation 4.2.1) in relation to dimensionless mass flow.

Equations 4.2.1 and 4.2.2 show the effect of the inlet temperature and pressure on the compressor performance. The limiting points on the performance map are the surge and choke limits.

Notice that the performance map is independent of inlet conditions if variables χ and Φ are used i.e. if dimensional variables are used, the map changes if the inlet conditions change. Usually the performance maps are presented for a given inlet state. If the inlet state is specified, χ is replaced by reference mass flow q_m, pressure ratio π may be replaced with the pressure increase in the compressor, and the dimensionless speed Φ by the reference speeds.

4.2.2 Combining compressor maps

The compressor maps in figures 4.1(a) and 4.1(b) are not useful when we would like to evaluate the performance of the whole process.The compressor maps need to be combined and to take in account the mass flow coming from the flash intercooler. To produce a single usable map of the whole process we build a dynamic model of the process and then varied the rotational speed of the compressor and the mass flow. The reference state for scaling is the inlet of the first compressor stage, after the returning flow has been mixed.

If the operational point was outside either of the original compressor maps it was not included in the process map i.e. the points were either compressor stage was in stall or surge were excluded.

4.3 Results

In this study the conditions of the design point are the same as in table 3.3.1.

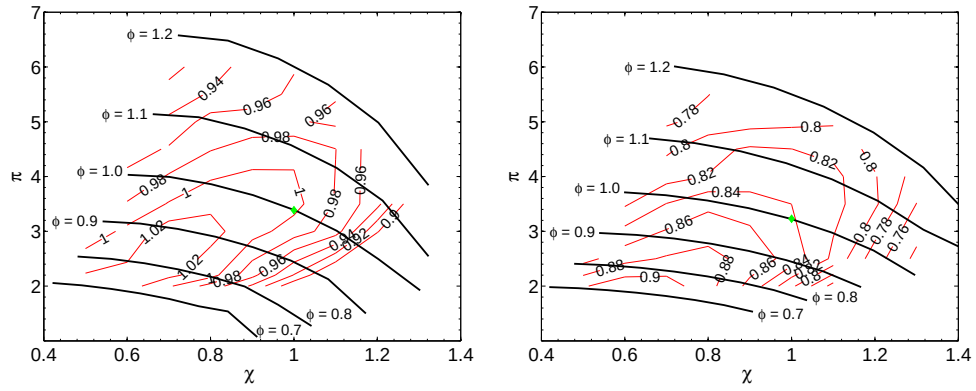

(a) (b)

Figure 4.3.1: Compressor maps of both the first (a) and the second(b) stage. Contours of isentropic efficiency divided by isentropic efficiency at the design point of the first stage, $\eta_{is}/\eta_{is,des,c1}$. The design point of the stage is indicated with a green diamond.

The compressor map of the first stage is shown in Fig. 4.1(a). The design operation point is indicated at the performance map with a green diamond marker. The design point is not located at the best efficiency point because the process is also required to operate at the low mass flows with reasonable efficiency. High efficiencies are obtained at lower pressure ratios and the operation range of the compressor is wide, which is typical for the centrifugal compressor with the vaneless diffuser. The trade off is that the efficiency of the design point is not as high as with vaned diffuser.

Fig. 4.1(b) shows the compressor performance map of the second stage. The map differs from the map of the first stage. The design principles with a two-stage compressor usually lead to a lower pressure ratio in the second stage. In addition, the compression performed in the first stage increases and the intercooling changes the density for the second stage in a manner that decreases the specific speed considerably. This optimisation usually lowers the efficiency as well Saari et al. (2008).

The combined process map is generated by calculating the process at the different operation points. The combined process map is shown in Fig. 4.3.2. The operation range is not as wide as the separate compressor maps would suggest. The reason for this is the change in pressure and temperature at the second stage inlet. The inlet condition of the second stage is a function

of the first stage operation, the pressure ratio and the efficiency, losses in the electrical motor and the flow from the flash intercooler. It can be stated that the limitation of the range in the lower end of the power range are mainly due to the surging of the second stage.

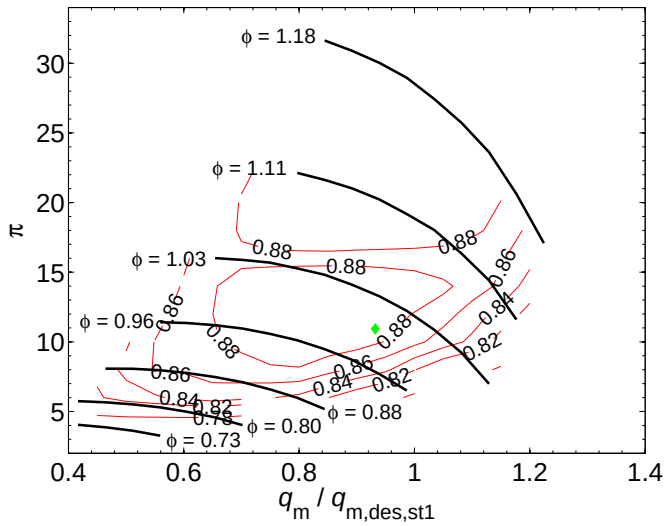

Figure 4.3.2: Combined compressor map. Contours of isentropic efficiency are made dimensionless and divided by isentropic efficiency at the design point of the first stage, $\eta_{is,pr}/\eta_{s,des,c1}$.

The condensation temperature is presented in figure 4.3(a) and the contours of the cooling power are plotted to the combined process map, which is shown in Fig. 4.3(b). At the design condensation temperature, the cooling power may vary from 0.65 to 1.15. At the higher and lower condensing temperatures (pressure ratio), the range of the cooling power is limited. In Figure 4.3(a), at lower condensation temperatures the available cooling powers are lower and at higher temperatures they are higher. As we assume that the heat exchanger remains the same the need for higher condensation pressure comes from higher atmospheric temperature. It is rather logical to think that higher atmospheric temperatures require larger cooling capacity. Thus, it is a desirable feature for a refrigeration system.

As there are no previous studies on the subject the validation of the results has to wait until the testing of the prototype is finished.

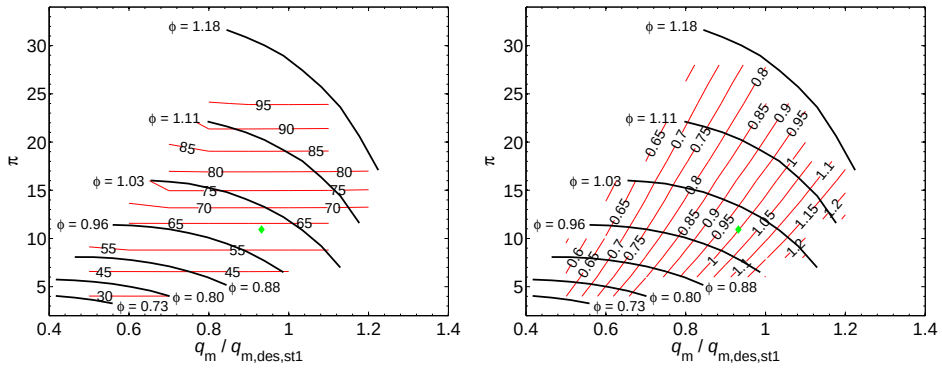

(a) (b)

Figure 4.3.3: Combined compressor map with (a) contours of condensing temperature and (b) contours of cooling power. Cooling power is divided by cooling power at design point.

Chapter 5

Effects of different impeller blade angle distributions on centrifugal compressor performance

One of the main challenges of realising the vapour cooling system with a centrifugal compressor is the design of the compressor stages. In the compressor all the work that is done on the fluid is done by the impeller. During the geometry design of the impeller, a design concept for degerming the optimal blade angle distribution which compares centrifugal compressor impeller channel loss development to the pressure loss development in a curved duct was found Came and Robinson (1998). In order to test how strong the correlation is three geometries were created with all other parameters constant except blade angle distribution.

The flow in a centrifugal compressor is very complicated, with strong three dimensional features. The design of centrifugal compressor impellers is widely covered in the literature, see e.g. Balje (1981); Came and Robinson (1998); Dixon (1989); Japikse (1996); Saravanamuttoo et al. (2001).

The inlet and outlet blade angles of impellers are normally determined in the initial one dimensional design phase. These angles define tangent of the blade camber line at inlet and outlet. Defining the blade angle for the whole length of the passage defines the shape of the blade camber line. This is called blade angle distribution.

In this paper, we create three different blade angle distributions, keeping all of the other parameters constant. This does not necessarily lead to optimal design, but illustrates the effects of the different distributions better.

The modern practise to determine the impeller blade angle distributions

is to calculate the compressible inviscid flow through the impeller passage and to determine the blade loading along the blade, and then to modify the meridional blade angle distribution to produce more favourable blade loading Zangeneh et al. (2004).

The meridional blade angle distribution has a significant effect on impeller efficiency. This phenomenon has been taken into account in the inverse design approach Zangeneh (1991, 1996); Zangeneh et al. (2004). In this method the desired blade loading, which is effectively static pressure difference between pressure and suction side, is predetermined and the geometry of the blade is designed to meet this initial criterium. However this design method has some drawbacks, as the resulting geometry is often mechanically complicated and the accuracy of the flow prediction methods available is poor. The flow in inverse design is usually solved as an inviscid compressible fluid with a uniform velocity distribution at the inlet. At the moment, a complete CFD analysis of a compressor stage is computationally too expensive.

Bonaiuti et al. Bonaiuti et al. (2006) have tried the design of experiments method to optimise transonic impeller. The compressor performance was modelled with CFD. A complete description of the design of experiment method is given by Montgomery (2004). Part of the research of Bonaiuti et al. involved finding the optimal meridional blade angle distribution for the inducer part of the impeller other geometrical features were also optimised. The optimised impeller showed consistent improvement of efficiency over the whole range. The parameters were optimised separately. They found that the hub meridional blade angle distribution had a greater effect on efficiency than the shroud meridional blade angle distribution.

The use of CFD in optimization is complicated. In general the shape of the objective function is not known and function noise is always present. This means that it is difficult to define the parameter subspace where global minimum occurs and furthermore, as the numerical methods add local minima that do not occur in the physical world the deterministic methods are often rendered useless. Here deterministic methods are understood as methods that select the next trial vector only by the information gained from the objective function so far usually this is done using derivatives. Thus the search algorithms have to be stochastic, although in some special applications deterministic methods have shown good results Giannakoglou and Papadimitriou (2008). The design of a centrifugal compressor geometry includes numerous variables and the performance has to be evaluated at different operational points. If the design parameters v are randomly varied at n points the search for optimum takes v^n evaluations. One high quality evaluation of a centrifugal compressor geometry takes hours of computational time

excluding the grid generation. Thus it is necessary to severely restrict the search space and to use sophisticated algorithms to accelerate convergence Van den Braembussche (2008). In order to do search space restriction effectively it is necessary to evaluate the influence of the different parameters to the performance of the compressor.

In this study the subject is the effect of blade angle distributions to the aerodynamic performance of the compressor stage. There are two main components in these losses, the friction losses at the walls and the losses caused by secondary flows. In practical centrifugal compressor designs the secondary flow losses are of greater importance. Equations for the secondary flows using intrinsic coordinates in turbomachinery have been developed by Horlock and Lakshminarayana Horlock and Lakshminarayana (1973); Lakshminarayana and Horlock (1973). The research articles on the secondary flows of centrifugal compressor impellers are numerous. The effect of geometric features on centrifugal compressor secondary flows were well explained in an article by Johnston (1998). The secondary flows in centrifugal impellers were further analysed by Brun and Kurz (2005).

5.1 Hypothesis

The theoretical basis of this study is that an impeller passage is considered as a rotating duct with an adverse relative velocity gradient of flow. The impeller in this study is shrouded. Now, the goal is to minimise the pressure loss by adjusting the meridional blade angle distribution without altering the blade angle at the impeller leading or trailing edge, as seen in Figure 5.2.1.

We are about to model pressure loss in this rotating duct, but the correlations we use are for non-rotating ducts. This is a source of some error. We shall use CFD calculations to examine the analogy between shape losses in non-rotating duct and in a shrouded centrifugal impeller is valid.

The pressure loss in such a duct comprises two elements, the pressure loss due to surface friction and the pressure loss due to the shape of the duct. To calculate the pressure loss due to skin friction we shall define the hydraulic diameter of the duct as

$$d_{\mathrm{h}} = 4\frac{A}{P}. \tag{5.1.1}$$

The hydraulic diameter is used to calculate the Reynolds number in the duct is

$$\mathrm{Re}_{\mathrm{dh}} = \frac{\rho|\mathbf{V}|d_{\mathrm{h}}}{\mu}. \tag{5.1.2}$$

Now, given that we know the relative roughness of the impeller, we can determine the friction coefficient of the wall from the *Colebrook-White* equation Kast (1988) as

$$\frac{1}{\sqrt{\xi}} = -2\lg\left[\frac{2.51}{\mathrm{Re}\sqrt{\xi}} + \frac{K_{\mathrm{rel}}}{3.71}\right]. \tag{5.1.3}$$

Where Re is the Reynolds number and K_{rel} is the relative surface roughness.

Now the pressure loss due to skin friction over the length of the channel l can be stated as

$$\Delta p = \int_l \xi \frac{\rho|\mathbf{V}|^2}{2} dl. \tag{5.1.4}$$

The integral form is essential, as the Reynolds number changes through the channel.

The pressure losses from the duct shape are due to the secondary flows induced by the geometry of the duct. The losses are higher if the turning angle is higher Kast (1988). The data by Kast (1988) suggests that at low turning angles, the turning radius does not play a significant role. Thus for low turning angles the shape loss is

$$k_{sl} = k\left(\Delta\beta\right). \tag{5.1.5}$$

Further we assume that there is linear dependency between the turning angle and the generated losses.

$$\frac{dk}{dl} = s\left|\frac{d\beta}{dl}\right| \tag{5.1.6}$$

where s is constant. This is clearly incorrect for wider ranges of $\Delta\beta$, but here we are interested only about one constant value of $\Delta\beta$. This is of importance because it is necessary, once again, to resort to the integral form to define the effects of shape loss.

$$\Delta p_{sl} = \int_l \frac{dk}{dl}\frac{\rho|\mathbf{V}|^2}{2} dl \tag{5.1.7a}$$

$$\Rightarrow \Delta p_{sl} = \int_l s\left|\frac{d\beta}{dl}\right|\frac{\rho|\mathbf{V}|^2}{2} dl \tag{5.1.7b}$$

This is necessary for the same reasons as in equation 5.1.4. It should be noted that now the total shape loss constant k is the same for the same difference of inlet and outlet angle regardless of the length of the bend if the bending happens only in one direction i.e. the derivative of the angle doesn't change sign. However, if the derivative of β changes sign in between the k_{sl} is larger for the same absolute value of angle change.

The velocity used to calculate the anticipated losses of different bends is computed assuming the lossless diffusion while fluid is considered as an ideal gas. This means that the fluid is considered inviscid and compressible.

As the longer channel induces larger losses, one could think that the shortest possible channel is the most efficient. This, however, is not the case in centrifugal compressors. Blade backsweep has been, without a doubt, proven superior over radial vanes Turton (1984). That is mainly due to a more radial outflow at the impeller exit, and thus, less work is done on tangential acceleration. If the blade angle turns radically at inlet, the length of the passage clearly increases. On the other hand, if the blade turns is very abruptly at the end to meet the desired backsweep, we lose the positive effects of the backsweep, as the flow will separate from the blade surface. The designer should be able to strike balance between these two effects.

The shape losses in a channel are usually contributed to three factors Vanyo (2003).

1. Flow separation at too sharp bends.

2. Secondary flow due to Ekman boundary layer flow phenomena

3. Görtler vortices at the wall.

The centrifugal force produces the Ekman boundary layer flow and Görtler vortices in a bend. In non-rotating bends the pressure gradient produced by centrifugal force is towards the concave side. In centrifugal compressors with backsweep in impeller, as in this case, the pressure gradient is away from the concave wall.

5.2 Methods

Three geometries were studied with the CFD solver Finflo in order to investigate the effect of the β-distributions presented in Figure 5.2.1. Effects of the turbulence model and grid density were also studied. All three geometries were modelled with three mass flows presented in table 5.2.1 that were not varied between cases.

Table 5.2.1: Mass flows used in modelling.

Low mass flow rate	$0.8\dot{m}_{des}$
Design mass flow	$\dot{m}_{des}$
High mass flow rate	$1.2\dot{m}_{des}$

5.2.1 Geometry cases

The compressor studied is a 2-D shrouded impeller consisting of an inlet part, 18 full blades and a parallel wall vaneless diffuser. The main design parameters of the compressor are shown in Table 5.2.2. The studied compressor is the second stage of a two-stage industrial compressor. This compressor is not intended for vapour cooling system, It operates with air. Unfortunately the actual inlet conditions are confidential.

Table 5.2.2: Main design parameters of the studied centrifugal compressor

Compressor pressure ratio	-	1.635
Mass flow rate	kg/s	3.045
Rotating speed	rpm	9600
d_2/d_3	-	0.616

Three different meridional blade angle distribution shapes, shown in Figure 5.2.1, are studied numerically. All geometries have similar inlet and outlet β-angles. The original distribution, referred later as case 1, is meridionally linear whereas the second distribution (case 2) turns more closer to the blade trailing edge and the third geometry (case 3) turns more closer to the blade leading edge. Surface grid of the impeller in case 1 without the shroud is shown in Figure 5.2.2, and every other gridpoint is visualised for the sake of clarity. All three grids consisted of three calculation blocks, which were inlet part, blade channel and diffuser. Every grid had the same amount of cells and similar node distribution, which made them comparable. In this context similar node distribution means that the same stretching laws and same distances of the first node from the wall was used.

Table 5.2.3: Absolute Lengths of impeller passages at midspan

Case 1	l_1
Case 2	1.03 l_1
Case 3	0.97 l_1

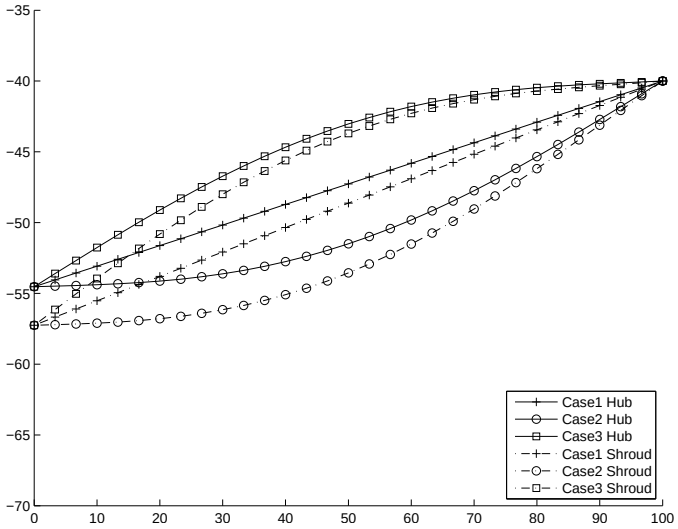

Figure 5.2.1: Meridional β-angle distribution of the studied compressor

5.2.2 Numerical methods

Finflo is a multi-grid Navier-Stokes solver employing the finite-volume method for spatial discretization. This study employs Roe's flux-difference splitting method Roe (1981) for inviscid fluxes. Convective fluxes are discretized by a second order upwind scheme, and also a flux limiter is applied for the studied problem.

Turbulence is modelled with the k-ω-SST model Menter (1993) in all cases and with Chien's k-ϵ model Chien (1982) in cases 1 and 2 and in the grid dependency study. Wall functions are not used.

The total enthalpy and momentum distributions are used as inlet boundary conditions, and the static pressure is extrapolated from the computational domain. Inlet flow conditions are from the one-dimensional design of the studied compressor. The static pressure is used as an outlet boundary condition. The mass flow difference between the inlet and outlet domains and the maximum change in density are used as convergence criteria.

5.2.3 Grid dependency

In order to evaluate the grid dependency of the studied geometry, three grid densities were compared: grid 1 had 68608 cells, grid 2 had 548864 cells and grid 3 has 932736 cells. The non-dimensional wall distance y^+ is less than unity in most of the blade surfaces for the two largest grids. The maximum value of y^+ 6.2 is located at the trailing edge of grid 3. The maximum value

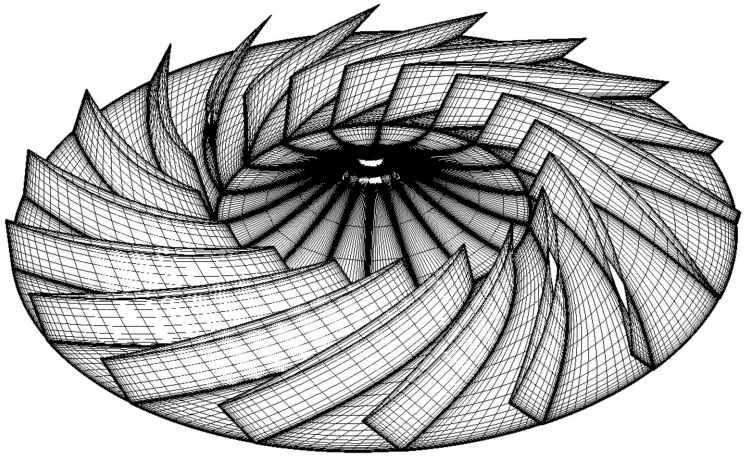

Figure 5.2.2: Surface grid of the impeller in case 1 without a shroud, every other gridline is visible for the sake of clarity. The impeller is presented as a whole, but the calculations were done using one flow passage.

for y^+ for the grid 1 at the blade surface was 7.4 on the trailing edge. The contours of y^+ for case 1 and a plot of y^+ at the blade pressure surface (white dots) at the design mass flow rate with the k-ω-SST turbulence model are shown in figure 5.2.3. Higher values of y^+ are seen at the leading and trailing edges. The values are higher at the pressure side (PS) than they are at the suction side (SS). Higher values than two are very rare, however this might have effect to the predicted wake and loss development as the viscous effects at the wall are underestimated if the values of y^+ are greater than one. The grid dependency was studied by looking at the flow angles at the impeller outlet and the total to static efficiency of the impeller and impeller-diffuser, $\eta_{\mathrm{s2,t-s}}$ and $\eta_{\mathrm{s3,t-s}}$ respectively. The comparisons were done at the design mass flow.

In the calculations, the specific isobaric heat capacity c_p was assumed constant, which is reasonable for air. Thus the efficiency for the impeller outlet can be defined as follows:

$$\eta_{s,t-s} = \frac{T_{2\mathrm{s}} - T_{\mathrm{t1}}}{T_2 - T_{\mathrm{t1}}}. \tag{5.2.1}$$

The static temperature after compression is calculated from the ideal gas equation.

$$T_{2\mathrm{s}} = T_{\mathrm{t1}} \left(\frac{p_2}{p_{\mathrm{t1}}} \right)^{\frac{R}{c_{\mathrm{p}}}} \tag{5.2.2}$$

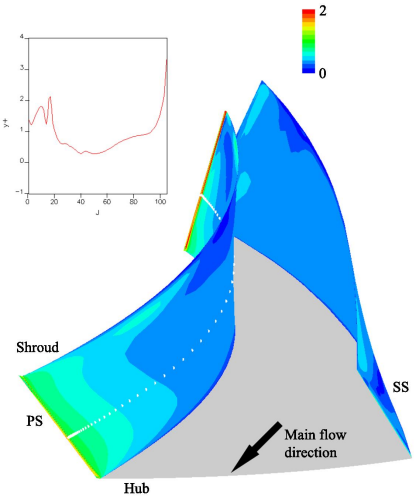

Figure 5.2.3: Contours of non-dimensional wall distance y^+ for case 1 at the design mass flow rate with the k-ω-SST turbulence model. Values at the pressure side (PS) are plotted from the leading edge to the trailing edge at highlighted white spots along the blade surface (J).

The efficiency and temperature at the diffuser outlet is defined correspondingly.

Based on Figure 5.4(a), the additional cells of grid 3 do not significantly affect the estimated efficiency when compared to grid 2. To confirm this, let us consider the flow angles at the impeller exit. From Figure 5.4(b) it is apparent that the flow angles in grids 2 and 3 are almost similar. From this, it can be interpreted that grid 3 with 932736 cells is sufficient, i.e. higher cell counts probably would not improve the results.

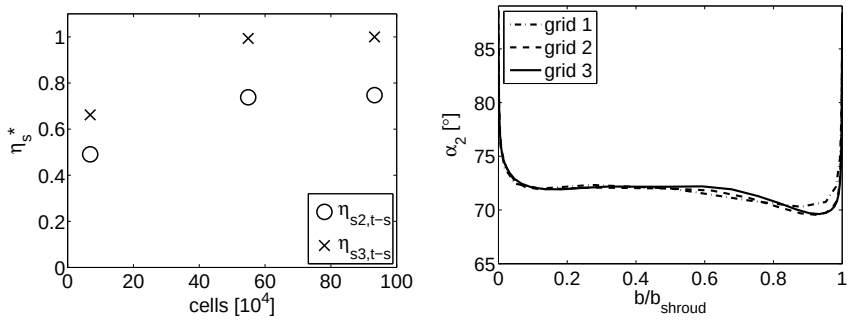

(a) (b)

Figure 5.2.4: Isentropic efficiency versus grid cell number (a) and flow angle at impeller outlet with different cell counts (b)

5.2.4 Assessment criterion

In addition to the efficiency presented before, the pressure loss coefficient and pressure rise coefficient are used to measure the performance of the diffuser. The total pressure loss coefficient K_p is

$$K_p = \frac{p_{t2} - p_{t3}}{p_{t2} - p_2}. \tag{5.2.3}$$

The total pressure loss coefficient gives information ot the quality of the diffuser flow.

The static pressure rise coefficient of the diffuser C_{pr} is

$$C_{\text{pr}} = \frac{p_3 - p_2}{p_{t2} - p_2}. \tag{5.2.4}$$

The pressure rise coefficient tells how much of the dynamic head at the impeller outlet was recovered as static pressure rise in the diffuser.

5.3 Results

Results calculated from the hypothesis

Inviscid compressible solutions for speed distribution in Figure 5.3.1 shows that case 2 has the highest average velocity and case 3 the lowest. As the flow passage is also the longest in case 2 the surface friction losses are the greatest, the relative values are presented in Table 5.3.1. The surface friction losses in Table 5.3.1 are calculated with equation 5.1.4 and the shape losses with equation 5.1.7. The only counter intuitive result is that case 3 seems to lose it's benefit of lower surface friction at off-design points. This would indicate that case 3 has lower total-to-total efficiency over the impeller, $\eta_{\text{t-t},2}$, than case 1 especially at off-design points.

From the figure 5.3.1 it can be seen that the turning the flow channel after diffusion provides better efficiency than if it was done before the diffusion occurs when considering shape losses according to the hypothesis.

5.3.1 Compressor performance

The total to static performances of the studied cases are presented in Figure 5.2(a). The first case has the best impeller efficiency at the design point, and consistently good efficiency at other points. Case 2 has the best performance at the low mass flow and case 3 at the high mass flow. The efficiencies are scaled to the maximum value of efficiency.

Table 5.3.1: Surface friction losses and shape losses in the impeller passages calculated according to the equations 5.1.4 and 5.1.7 with different mass flows scaled to the losses at design mass flow values of case 1.

$0.8\dot{m}_{des}$	Surface friction	Shape loss
Case 1	0.71	0.64
Case 2	0.89	0.62
Case 3	0.68	0.68
$\dot{m}_{des}$	Surface friction	Shape loss
Case 1	1	1
Case 2	1.25	0.97
Case 3	0.94	1.06
$1.2\dot{m}_{des}$	Surface friction	Shape loss
Case 1	1.32	1.44
Case 2	1.60	1.39
Case 3	1.32	1.53

At low mass flow the stage efficiency differences are larger than the impeller efficiency differences. Although case 1 has the best impeller efficiency at the design point, case 3 has practically the same stage efficiency at the same point.

At the high mass flow rate, the impeller efficiencies of case 1 and 3 are practically similar, but the stage efficiency of case 3 is slightly higher.

Impeller total to total efficiencies are presented in Figure 5.2(b). The efficiency of case 1 is highest at the low and design mass flows. Case 2 has the lowest efficiency at the high and design mass flows, but is practically equal to the highest efficiency at the low mass flow. Also, case 3 has clearly the lowest total-to-total efficiency at the design point, but does better at off-design values. This directly contradict the results calculated based on the hypothesis.

5.3.2 Losses in the impeller

Table 5.3.2 presents the work done in the impeller passage at the design mass flow. All values are scaled to the work done in Case 1. The losses are calculated and the percentage of losses caused by the turbulent dissipation and the viscous dissipation at the wall are presented. The loss distributions between cases are very similar. The work done is calculated between total

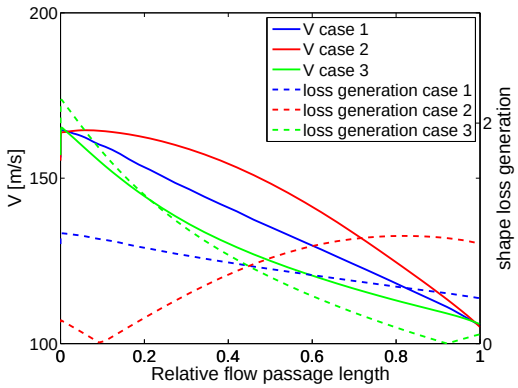

Figure 5.3.1: Velocity distribution of inviscid compressible flow at design mass flow as a function of passage length and the calculated shape loss generation based on these velocities.

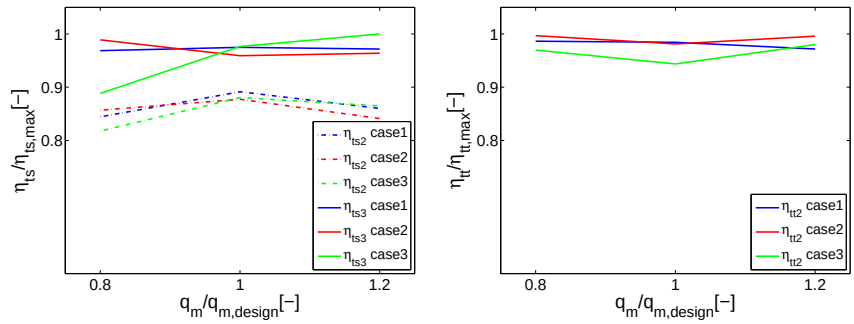

(a) (b)

Figure 5.3.2: Isentropic total to static efficiencies (a) and isentropic total to total efficiencies over impeller (b) as a function of mass flow. The efficiencies are confidential and are presented relative to the maximum value.

states. As no heat is conducted through the walls this includes all the work done to the fluid by the impeller.

5.3.3 Velocity profiles

In Figure 5.3.3, the relative velocity profiles in the flow passages are presented under the design mass flow conditions. Case 2 differs in the shape of the curve as the flow starts to accelerate early in the passage. The average relative velocity is the highest in case 2 and the lowest in case 3.

Also the velocities modelled with the k-ϵ turbulence model for case 1 and 2 are presented in Figure 5.3.3. They are 5-10% higher than the ones

Table 5.3.2: Losses in the impeller passage

	case 1	case 2	case 3
W_2	1.000	0.983	1.004
W_{2s}	0.932	0.901	0.935
W_{losses}	0.072	0.087	0.074
Losses			
Viscous	15.8 %	15.8 %	13.4 %
Turbulence	21.4 %	21.8 %	19.6 %

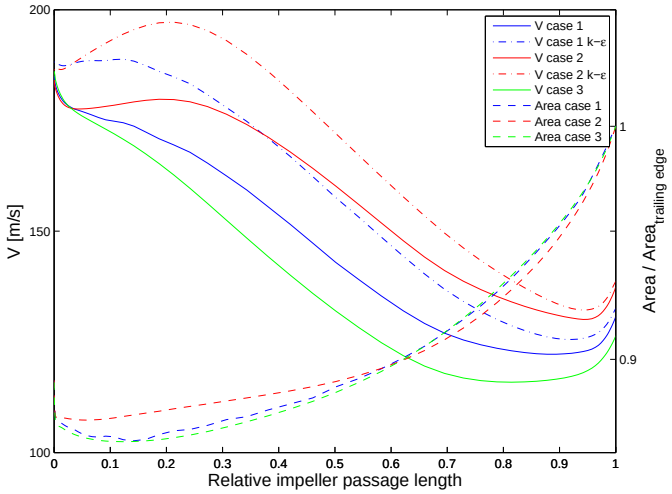

Figure 5.3.3: Mass flow averaged flow velocity relative to the impeller at the flow passage and the development of the cross sectional area of the flow passage.

modelled with k-ω, and the curve shape is also different.

The simulated flow fields through all three of the considered impeller channels (figure 5.4(a)) display an increase in the mass-flow-averaged velocity near the trailing edge, even if the cross-sectional area steadily increases from the inlet to the outlet. This has to be due to flow separation that decreases the effective cross sectional area. In the flow field figures , 5.4(b) and 5.4(c) we see a large area of low energy wake flow close to the trailing edge at the suction side of the impeller, as can be expected. The contours of relative velocity also confirm the higher averaged velocities of case 2 over cases 1 and 3.

Figure 5.3.5 shows the mass averaged flow angle of all cases along the passage alongside the actual blade angles at the hub and shroud. The flow turns the most in case 3 and the least at case 2. These results are calculated

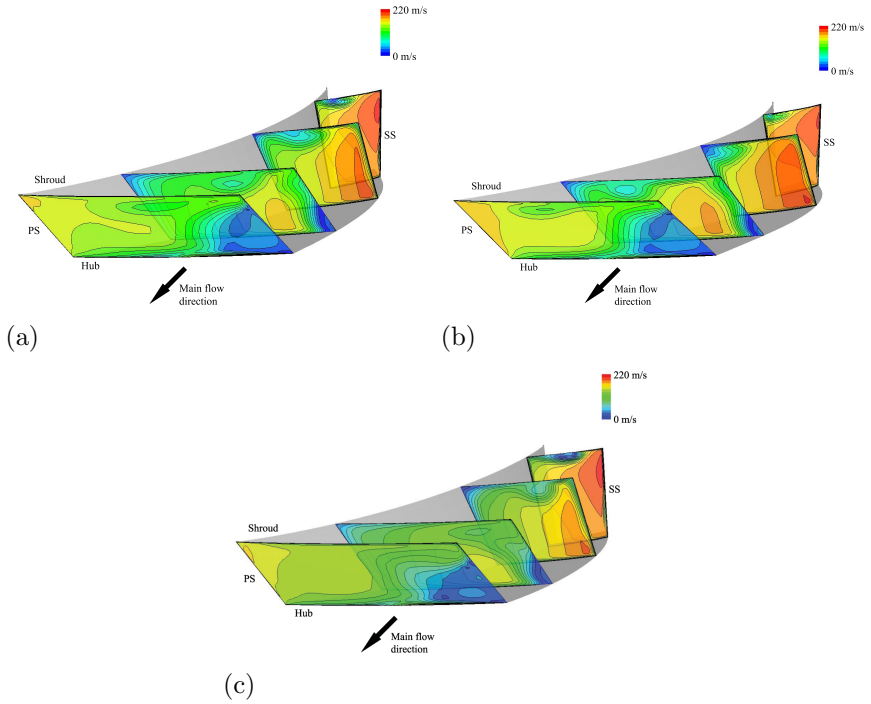

Figure 5.3.4: Contours of relative velocity in the impeller for (a) case 1, (b) case 2 and (c) case 3

at design mass flow.

Figures 5.3.3 and 5.3.5 show that the actual beta angle changes quickly after the channel area starts to grow more rapidly. This is due to flow separation, based on Figure 5.3.4.

The flow field shows expected behaviour for a centrifugal compressor. The high energy jet flow is near the pressure side, and the low energy wake is on the suction side. Similar results can be seen in Iancu et al. (2007).

In Figure 5.3.4 cases 1 and 3 show clear low energy flows near the leading edge at the shroud, unlike case 2. This is due to flow separation. However, case 2 shows the highest mass averaged velocity in Figure 5.3.3.

5.3.4 Blade loading

Here blade loading is defined as the difference of static pressure between the pressure side and suction side surface. It describes how much work the impeller does on the fluid at the given point. In Figure 5.3.6, the blade loading of case 2 near the leading edge is considerably lower than in other cases and is highest at the trailing edge. The opposite is true for case 3.

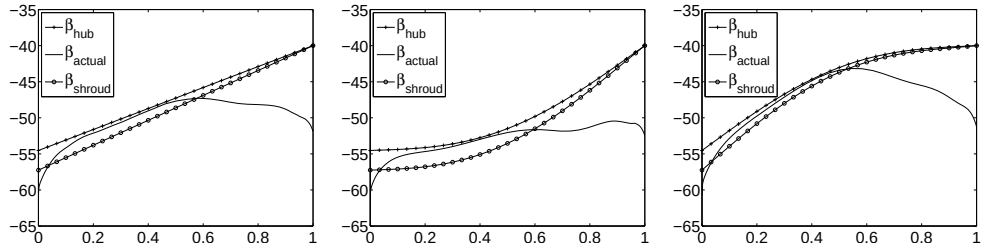

(a) (b) (c)

Figure 5.3.5: The actual mass averaged flow angles in the impeller versus the blade angles at hub and shroud (a) case 1 (b) case 2 (c) case 3

Using common terminology in turbomachinery it can be said that case three is front loaded and case 2 aft-loaded. Case 1 shows small wobbling near the leading edge.

5.3.5 Diffuser performance

The diffuser performance is measured by the recovery of the dynamic pressure to static pressure and by the loss of total pressure as described in section 5.2.4. The pressure rise coefficient of the diffuser of Case 3 is the lowest at the low mass flow rate, but the highest at other points. Cases 1 and 2 have their lowest pressure rise coefficients at the design mass flow.

The overall total pressure loss coefficient is higher at lower mass flow rates. This indicates that the diffusion is too abrupt at the design mass flow. Thus, more sophisticated diffuser design would increase stage efficiency.

Table 5.3.3: Diffuser performance

	case 1		case 2		case 3	
	C_{pr}	K_{p}	C_{pr}	K_{p}	C_{pr}	K_{p}
Low mass flow	0.180	0.452	0.196	0.417	0.100	0.510
Design mass flow	0.125	0.415	0.125	0.403	0.145	0.366
High mass flow	0.173	0.320	0.198	0.292	0.208	0.268

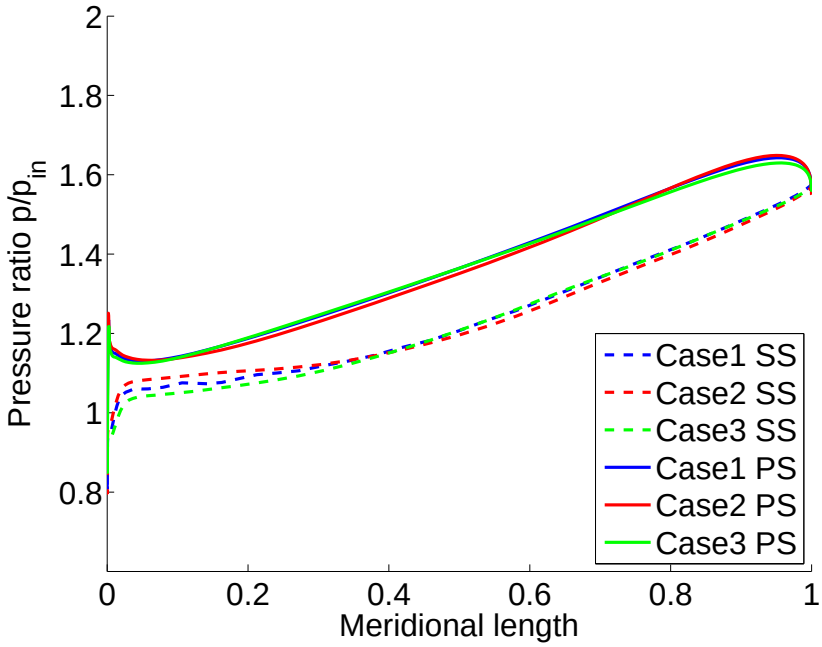

Figure 5.3.6: The ratio of the static pressure to the pressure at the inlet at the midspan of the flow channel on both the suction and pressure sides at design mass flow

Chapter 6

Discussion on research

The goal of our research group in the project was to produce a design of a vapour cooling system utilising centrifugal compressor for jetliners. This thesis presents a part of the studies done to meet the objective, concerning mostly thermal and aerodynamic efficiency of the system. The design was done and a prototype of the system was build on the basis of the design. At the time of writing the prototype is under testing.

The feasibility of different working fluids for vapour cooling system utilising two stage centrifugal compressor without intercooling was assessed. For this application, with given environmental and security restrictions, the R245fa and R134a were the only good candidates for the working fluid. However, if the requirement of non-flammability could be relaxed we could probably achieve less overall global warming through better efficiency with hydrocarbons. In well maintained machines the GWP of the fluid is not the main environmental concern, at least during machines service life.

Why do the other interesting fluids fail? Ammonia is not feasible in this size range, as it has high volumetric evaporation heat and thus too small volumetric flow through the compressor. Water has triple point just above 0 °C, so it is automatically excluded from the intended temperature range, and with evaporation temperature of 5 °C it would still produce too low evaporating pressure for feasible mechanical design. Carbon dioxide is an interesting fluid for refrigeration, but isn't suited for this application due to its high evaporating and condensing pressure. It would be worthwhile to investigate it's use in a similar vapour cooling cycle in the future.

The refrigeration process using the two-stage centrifugal compressor and the flash intercooler was modelled and optimised based on the COP value. The compressor's electric motor is cooled with the refrigerant. Two different refrigerants were used, R134a and R245fa. These refrigerants were used because a preliminary study indicated that the approximate COP was fairly

good. Moreover, they are non-toxic and non-flammable, and they have a relatively low GWP and zero ODP. A simplified real-gas model was used in modelling to as it was simple to implement.

The pressure ratio of the compressor is approximately same in both compressor stages with R245fa at the optimum operation point of the cycle. With R134a, the pressure ratio of the second stage is slightly higher. Furthermore, the optimum efficiency of the overall cycle is not at the point of the optimum efficiency of either compressor stage. The losses at the electric motor cooling crucially affect the overall efficiency of the cycle.

The modest values for COP are explained by the quite large temperature difference between evaporation and condensation. Generally, it should be stressed that the COP is valid criteria of comparison only between cycles operating with the same evaporation and condensation temperature and cooling power requirement.

Based on these studies, R245fa was selected as the working fluid. The geometry of the compressor stages was created. The performance was modelled by CFD and corrections to the geometry were done based on these results. After some iterations the geometry was finished and the compressor maps calculated for the final design. These maps were used for the off-design performance modelling of the vapour cooling cycle.

The COP values obtained at the off-design calculations are rather constant in respect to the mass flow and thus cooling capacity at a constant condensing temperature (pressure ratio of the whole compressor) and therefore, high performance is maintained with a wide range of cooling power. Also a higher pressure ratio and thus a greater temperature difference between condenser and evaporator lead to lower COP values, which is expected.

The observed operation range is wide and COP values rather invariable over a larger range of cooling powers at a constant evaporation temperature.

In the process it was also found that the high speed centrifugal compressor provides a feasible alternative to a displacement compressor in the residential scale cooling applications. Furthermore, the ability to control the pressure ratio increases the comfort of the cooling as the temperature of the evaporation can be controlled.

The performance of the cycle is good, but it suffers from the high relative tip clearance of the impeller. This is due to small impeller size and bearings required to accommodate the high rotational speeds. The refrigeration system was not optimised with respect to the overall fuel consumption of the jetliner. In future studies it would be interesting to optimise the size of the heat exchangers with respect to the overall fuel consumption as larger heat exchanger would increase the system efficiency but also increase the fuel consumption due to the added weight.

A theory that the secondary flow losses in centrifugal compressor impeller behave similarly to the losses in a curved duct was suggested. The results of the CFD simulations done seemed to disagree with the theory as the relative efficiencies between cases was not the same as predicted by the hypothesis. In retrospect this is not surprising. The most important components of the secondary flows are strongly affected by centrifugal force. Centrifugal force acts in the opposite direction in backswept impeller channels than in irrotational curved ducts.

The research presented in chapter 5 opens up many interesting questions. As the secondary flows in a rotating duct is strongly governed by centrifugal force it should be possible to predict the effect of design features such as the meridional blade angle distribution if we are able to predict the development of the boundary layers in rotating systems. Some research on the subject has been done but it is not widely applied in turbomachinery.

6.0.6 Suggestions for further research

To reliably asses whether the vapour cooling system should be employed in jetliners the overall effect of the system to the fuel economy should be assessed. It is likely that the generation of electric power that runs the vapour cooling cycle is more efficient than taking the bleed flow from the jet engine compressor to power the air cycle machine. An important factor to consider is also the weight of the power electronics, and research to reduce their weight should be done.

As suggested before, employing this type of system in residential air conditioning is highly recommendable, as it provides more comfortable cooling with wide control range and high efficiency. Enormous amounts of electric energy is already used for air conditioning and refrigeration and as the standard of living will rise in the countries near the equator more cooling capacity will certainly be installed. As it is unlikely that the developing countries will produce the electric energy needed to operate cooling systems from renewable sources or with nuclear power the increase of cooling capacity will lead to an increase of CO_2 emissions and will thus contribute to global warming, the biggest environmental threat of our times. Therefore, it would be important to make commercially available cooling systems that have good efficiency with low initial cost. Thus research on producing cheap, small scale vapour cooling cycles with high efficiency is highly recommended. The most important research subjects to lower the costs of refrigeration system utilising high-speed centrifugal compressors are producing cheaper impellers, bearings and power electronics.

The research done in chapter 5 concentrates on the question how could

the centrifugal compressor impeller losses be calculated from inviscid solutions of the flow. The suggested analogy is clearly too simple. However, combining the results of Horlock and Lakshminarayana (1973) with common theories of boundary layer development and the solution of inviscid flow calculations of the flow passage, a calculation routine to predict these losses could be found. This routine would very likely be faster than Reynolds averaged solution of the Navier-Stokes equations (RANS) commonly used in CFD. This calculation routine could be used in optimisation to go through considerably larger design space than is possible today with RANS calculations. After the parameter sub-space where the most efficient designs can be found is identified with the method described above an optimisation routine described by Van den Braembussche (2008) could be run. The advantages of the method would be larger search space of parameters and faster convergence of the solution.

Appendix A

Publication I

Röytta P., Honkatukia J. and Turunen-Saaresti T. **Centrifugal Compressor Working Fluids for Refrigeration Cycle**

Reprinted from
Proceedings of ASME Turbo Expo 2009,

Appendix B

Publication II

Röytta P., Honkatukia J. and Turunen-Saaresti T. **Optimising the refrigeration cycle with a two-stage centrifugal compressor and a flash intercooler.**

Reprinted from
International Journal of Refrigeration, Volume 32, Issue 6, September 2009, Pages 1366-1375,

Appendix C

Publication III

Röytta P., Honkatukia J. and Turunen-Saaresti T. **Predicting off-design range and performance of refrigeration cycle with two-stage centrifugal compressor and flash intercooler.**
International Journal of Refrigeration,
Submitted for publication, 2009,

Appendix D

Publication IV

Röytta P., Grönman A., Jaatinen A., Turunen-Saaresti T. and Backman J.
Effects of different blade angle distributions on centrifugal compressor performance
International Journal of Rotating machinery,
Submitted for publication, 2009,

Bibliography

Aprea, C., Mastrullo, R., Renno, C., 2006. Experimental analysis of the scroll compressor performances varying its speed. Journal of Applied Thermal Engineering 26, 983–992.

Aprea, C., Mastrullo, R., Renno, C., 2008. Determination of the compressor optimal working conditions. Applied Thermal Engineering.

Arkkio, A., Jokinen, T., Lantto, E., September 2005. Induction and permanent-magnet synchronous machines for high-speed applications. Vol. 2. pp. 871–876 Vol. 2.

Balje, O. E., 1962. A study on design criteria and matching of turbomachines: Part b – compressor and pump performance and matching of turbocomponents. ASME J. Eng. Gas Turbines Power 84, 103–114.

Balje, O. E., 1981. Turbomachines : a guide to design, selection and theory. Wiley, New York.

Bein, T., Lee, Y., 1999. Performance evaluation of an air-conditioning compressor part i: Measurement and design modeling. International Journal of Rotating Machinery 5 (4), 231–240.

Bonaiuti, D., Arnone, A., Ermini, M., Baldassarre, L., 2006. Analysis and optimization of transonic centrifugal compressor impellers using the design of experiments technique. Journal of Turbomachinery 128, 786.

Brown, J. S., Dec. 2007. Predicting performance of refrigerants using the peng-robinson equation of state. International Journal of Refrigeration 30 (8), 1319–1328.

Browne, M. W., Bansal, P. K., 8 1998. Steady-state model of centrifugal liquid chillers. International Journal of Refrigeration, 21 (5), 343–358.

Brun, K., Kurz, R., 2005. Analysis of secondary flows in centrifugal impellers. International Journal of Rotating Machinery 2005 (1), 45–52.

Calm, J., 2002. Options and outlook for chiller refrigerants. International Journal of Refrigeration 25 (6), 705–715.

Calm, J., Hourahan, G., 2001. Refrigerant data summary. Engineered Systems 18 (11), 74–88.

Calm, J. M., Aug. 2006. Comparative efficiencies and implications for greenhouse gas emissions of chiller refrigerants. International Journal of Refrigeration 29 (5), 833–841.

Came, P., Robinson, C., 1998. Centrifugal compressor design. Vol. 213. Prof Eng Publishing, pp. 139–155.

Casey, M., April 1985. The effects of reynolds number on the efficiency of centrifugal compressor stages. Journal of Engineering for Gas Turbines and Power 107, 541 – 548.

Chen, J., Chen, X., Wu, C., 11 2002. Ecological optimization of a multistage irreversible combined refrigeration system. Energy Conversion and Management, 43 (17), 2379–2393.

Chien, K., 1982. Predictions of channel and boundary-layer flows with a low-reynolds-number turbulence model. AIAA Journal 20 (1), 33–38.

Cho, H., Chung, J. T., Kim, Y., 2003. Influence of liquid refrigerant injection on the performance of an inverter-driven scroll compressor. International Journal of Refrigeration 26, 87–94.

Cuevas, C., Lebrun, J., 2009. Testing and modelling of a variable speed scroll compressor. Applied Thermal Engineering 29, 469–478.

d'Accadia, M. D., de Rossi, F., 1998. Thermoeconomic optimization of a refrigeration plant. International Journal of Refrigeration, 21 (1), 42–54.

Dixon, S. L., 1989. Fluid mechanics, thermodynamics of turbomachinery, 3rd Edition. Pergamon Press, Oxford, in SI/metric units.

Giannakoglou, K. C., Papadimitriou, D. I., 2008. Optimization and Computational Fluid Dynamics. Springer-Verlag, Ch. Adjoint Methods for Shape Optimization, pp. 79–109.

Gordon, J. M., Ng, K. C., Chua, H. T., 1995. Centrifugal chillers: thermodynamic modelling and a diagnostic case study. International Journal of Refrigeration 18, 253.257.

Guo-liang, D., 11 2007. Recent developments in simulation techniques for vapour-compression refrigeration systems. International Journal of Refrigeration, 30 (7), 1119–1133.

Horlock, J., Lakshminarayana, B., 1973. Secondary flows: Theory, experiment, and application in turbomachinery aerodynamics. Annual Reviews in Fluid Mechanics 5 (1), 247–280.

Iancu, F., Trevino, J., Sommer, S., 2007. Numerical Analysis of Blade Geometry Generation Techniques for Centrifugal Compressors. International Journal of Rotating Machinery 2007, article ID 48683, 7 pages.

Japikse, D., 1996. Centrifugal compressor design and performance. Concepts ETI, cop, Wilder (VT).

Johnston, J., 1998. Effects of system rotation on turbulence structure: A review relevant to turbomachinery flows. International Journal of Rotating Machinery 4 (2), 97–112.

Kast, W., 1988. VDI-Wärmeatlas : Berechnungsblätter für den Wärmeübergang, 5th Edition. Verein Deutscher Ingenieure, Düsseldorf, Ch. Druckverlust, pp. La1 – Lc9.

Koury, R. N. N., Machado, L., Ismail, K. A. R., 2001. Numerical simulation of a variable speed refrigeration system. International Journal of Refrigeration 24, 192–200.

Kuosa, M., 1994. Kylmäkoneprosessin laskenta ympäristöystävllisellä väliaineella. Master's thesis, Lappeenranta University of Technology, Lappeenranta, format: kirja; Language of Abstract: eng.

Kuosa, M., Backman, J., Talonpoika, T., Sallinen, P., Larjola, J., Honkatukia, J., June 1998. Refrigeration process with high speed technology. In: Proceedings of the International Gas Turbine & Aeroengine Congress & Exhibition. ASME.

Kuosa, M., Sallinen, P., Larjola, J., Aug. 2004. Numerical and experimental modelling of gas flow and heat transfer in the air gap of an electric machine. Journal of Thermal Science 13 (3), 264–278.

Kuosa, M., Sallinen, P., Reunanen, A., Backman, J., Larjola, J., Koskelainen, L., Mar. 2005. Numerical and experimental modelling of gas flow and heat transfer in the air gap of an electric machine. part ii: Grooved surfaces. Journal of Thermal Science 14 (1), 48–55.

Lakshminarayana, B., Horlock, J., 1973. Generalized expressions for secondary vorticity using intrinsic co-ordinates. Journal of Fluid Mechanics 59 (01), 97–115.

Lemmon, E., Huber, L., McLinden, M., April 2007. NIST Reference Fluid Thermodynamic and Transport Properties - REFPROP Version 8.0 User's Guide. National Institute of Standards and Technology, Boulder, Colorado 80305.

Lucas, K., 1988. VDI-Wärmeatlas : Berechnungsblätter für den Wärmeübergang, 5th Edition. VDI-Verlag, Düsseldorf, Ch. Berechnungsmethoder für Stoffeigenschaften, pp. Da1 – Da36.

Menter, F., 1993. Zonal two-equation $k - \omega$ turbulence models for aerodynamic flows. In: AIAA Paper 93-2906.

Montgomery, D. C., 2004. Design and Analysis of Experiments. John Wiley & Sons, Inc.

Münzberg, H., Kurzke, J., 1977. Gasturbinen-Betriebsverhalten und Optimierung. Springer-Verlag.

Musgrave, D. S., March 1980. The prediction of design and off-design efficiency for centrifugal compressor impellers. In: Performance prediction of centrifugal pumps and compressors; Proceedings of the Twenty-fifth Annual International Gas Turbine Conference and Exhibit and Twenty-second Annual Fluids Engineering Conference. New Orleans, La, United States, pp. 185 – 189.

Roe, P. L., 1981. Approximate Riemann solvers, parameter vectors and difference schemes. Journal of Computational Physics 43, 357–372.

Röyttä, P., Turunen-Saaresti, T., Honkatukia, J., 2009. Optimising refrigeration cycle with two-stage centrifugal compressor and flash intercooler. International Journal of Refrigeration 32, 1366–1375.

Saari, J., 1998. Thermal analysis of high-speed induction machines. Ph.D. thesis, Helsinki University of Technology.

Saari, J., Backman, J., Peussa, J., 2008. Conceptual design of a multistage high-speed motor driven air compressor. In: Proceedings of ASME Turbo Expo 2008: Power for Land, Sea and Air.

Saleh, B., Wendland, M., Mar. 2006. Screening of pure fluids as alternative refrigerants. International Journal of Refrigeration 29 (2), 260–269.

Saravanamuttoo, H., Rogers, G., Cohen, H., March 2001. Gas Turbine Theory, 5th Edition. Prentice Hall.

Solomon, S., Qin, D. (Eds.), 2007. IPCC (Intergovernmental Panel for Climate Change). Climate Change 2007: The Physical Science Basis. Contribution of Working Group I to the fourth Assesment Report of the International Panel on Climate Change. Cambridge University Press.

Spence, S. W., Doran, W. J., Artt, D. W., McCullough, G., 2005. Performance analysis of a feasible air-cycle refrigeration system for road transport. International Journal of Refrigeration 28 (3), 381 – 388.

Spence, S. W. T., Doran, W. J., Artt, D. W., 2004. Design, construction and testing of an air-cycle refrigeration system for road transport. International Journal of Refrigeration 27 (5), 503 – 510.

Talonpoika, T., March 1994. Modelling the properties of fluid in a thermodynamic cycle. Research report EN B-82, Lappeenranta University of Technology, Lappeenranta, in Finnish.

Traupel, W., 1966. Thermal Turbomachines. (In German). Vol. 1- Thermodynamics and Fluid-Mechanics Calculations. Springer-Verlag, Berlin.

Turton, R. K., 1984. Principles of Turbomachinery. E. & F. N. Spon Ltd.

Ust, Y., Sahin, B., 5 2007. Performance optimization of irreversible refrigerators based on a new thermo-ecological criterion. International Journal of Refrigeration, 30 (3), 527–534.

Vaidyaraman, S., Maranas, C. D., 1999. Optimal synthesis of refrigeration cycles and selection of refrigerants. AICHE Journal 45 (5), 997–1017, cP: Copyright Ã‚Â© 1999 American Institute of Chemical Engineers (AIChE); PN: 0001-1541.

Van den Braembussche, R., 2008. Optimization and Computational Fluid Dynamics. Springer-Verlag, Ch. Numerical Optimization for Advanced Turbomachinery Design, pp. 147–189.

Vanyo, J. P., March 2003. Rotating Fluids in Engineering and Science, illustrated edition Edition. Dover Publications Inc.

Wang, X., Yuan, X., 2007. Reuse of condensed water to improve the performance of an air-cycle refrigeration system for transport applications. Applied Energy 84 (9), 874–881.

Wilson, D. G., 1988. The design of high-efficiency turbomachinery and gas turbines. MIT Press, Cambridge, MA.

Winkler, J., Aute, V., Radermacher, R., 2008. Comprehensive investigation of numerical methods in simulating a steady-state vapor compression system. International Journal of Refrigeration 31, 930–942.

Zangeneh, M., 1991. A compressible three-dimensional design method for radial and mixed flow turbomachinery blades. International Journal for Numerical Methods in Fluids 13 (5), 599–624.

Zangeneh, M., 1996. Inverse design of centrifugal compressor vaned diffusers in inlet shear flows. Journal of Turbomachinery 118, 385.

Zangeneh, M., Schleer, M., Pløger, F., Hong, S., Roduner, C., Ribi, B., Abhari, R., 2004. Investigation of an Inversely Designed Centrifugal Compressor Stage - Part I: Design and Numerical Verification. Journal of Turbomachinery 126, 73.